Redox Biology 81 (2025) 103530

Contents lists available at ScienceDirect

Redox Biology

journal homepage: www.elsevier.com/locate/redox

Oxidative stress-mediated abnormal polarization of decidual macrophages promotes the occurrence of atonic postpartum hemorrhage

Jiangxue Qu [a,b,c,1], Hai Jiang [a,b,c,1], Boyang Zhang [d], Huifeng Shi [a,b,c], Shuai Zeng [a,b,c], Wei Wang [d,**,2], Lian Chen [a,b,c,***,2], Yangyu Zhao [a,b,c,*,2]

[a] Department of Obstetrics and Gynecology, Peking University Third Hospital, Beijing, China
[b] National Clinical Research Center for Obstetrics and Gynecology (Peking University Third Hospital), Beijing, China
[c] National Center for Healthcare Quality Management in Obstetrics, Beijing, China
[d] Department of Immunology, School of Basic Medical Sciences, NHC Key Laboratory of Medical Immunology, Medicine Innovation Center for Fundamental Research on Major Immunology-related Diseases, Peking University, Beijing, China

ARTICLE INFO

Keywords:
Atonic postpartum hemorrhage
Macrophage polarization
Oxidative stress
Cytokines
Uterine contraction-associated proteins

ABSTRACT

Postpartum hemorrhage (PPH) is the leading cause of maternal mortality worldwide. However, the mechanism underlying atonic PPH remains partially elucidated. Multi-omics revealed that differentially expressed proteins and metabolites were enriched in the immune-inflammation pathway in the vaginal blood of patients with atonic PPH. There was a pro-inflammatory immune microenvironment primarily activated by M1 macrophages in the decidua of the patients with atonic PPH, which presented as increased tumor necrosis factor (TNF)-α, interleukin (IL)-6, and IL-8 levels and affected the contraction of the uterine smooth muscle. Besides, the decidual macrophage of the atonic PPH group exhibited increased oxidative stress. The PPH decidual cell culture medium induced the polarization of peripheral blood monocytes towards M1 macrophages while markedly increasing the levels of reactive oxygen species and superoxide anion radical. Using hydrogen peroxide (H_2O_2) to stimulate decidual macrophages induced a similar polarization state to that in atonic PPH samples, and the secretion of pro-inflammatory cytokines, such as TNF-α and IL-8, was significantly upregulated, which markedly impacted the expression of contraction-associated proteins (CAPs) in the uterine smooth muscle cells (uSMCs). The animal model suggested that H_2O_2 promoted the polarization of placental macrophages towards M1, affecting the levels of placental oxidative stress and inflammatory infiltration, and the contractility of uterine smooth muscle tissues.

Abbreviations: PPH, Postpartum hemorrhage; TNF-α, tumor necrosis factor-α; IL, interleukin; H_2O_2, hydrogen peroxide; CAPs, contraction-associated proteins; uSMCs, uterine smooth muscle cells; COX-2, cyclooxygenase-2; OTR, oxytocin receptor; CCL-2, C C motif ligand 2; MIP, macrophage inflammatory protein; MCP, monocyte chemotactic protein; ROS, reactive oxygen species; BMI, body mass index; HDP, hypertension disorders of pregnancy; GDM, gestational diabetes mellitus; GO, Gene Ontology; KEGG, Kyoto Encyclopedia of the Genome; MMP2, Matrix Metallopeptidase 2; MMP9, Matrix Metallopeptidase 9; α-SMA, α-Smooth muscle actin; TAGLN, Transgelin; Basic FGF, basic fibroblast growth factor; GM-CSF, granulocyte-macrophage colony stimulating factor; CTACK, cutaneous T cell-attracting chemokine; G-CSF, granulocyte-colony stimulating factor; GRO-a, growth-regulated oncogene-alpha; HGF, hepatocyte growth factor; IFN, interferon alpha; LIF, leukemia inhibitory factor; M-CSF, macrophage colony stimulating factor; MIG, monokine induced by IFN-g; RANTES, regulate upon activation normal T cell expressed and secreted; SCF, stem cell factor; SDF-1α, stromal cell-derived factor 1α; SDF-1α, stromal cell-derived factor-alpha; TNF, tumor necrosis factor; TRAIL, tumor necrosis factor-related apoptosis-induced ligand; β-NGF, beta-nerve growth factor; NK, natural killer; T cells, T lymphocytes; 8-OHdG, 8-hidroxy-2-deoxyguanosine; SOD, superoxide anion radical dismutase; GPX3, glutathione peroxidase 3; iNOS, inducible nitric oxide synthase; Arg-1, arginase-1; CD86, cluster of differentiation 86; CD206, cluster of differentiation 206.

* Corresponding author. Prof. Yangyu Zhao: Department of Obstetrics and Gynecology, Peking University Third Hospital; National Clinical Research Center for Obstetrics and Gynecology (Peking University Third Hospital); National Center for Healthcare Quality Management in Obstetrics, 100191, Beijing, China.

** Corresponding author. Prof. Wei Wang: Department of Immunology, School of Basic Medical Sciences, Peking University, NHC Key Laboratory of Medical Immunology (Peking University), 100191, Beijing, China.

*** Corresponding author. Prof. Lian Chen: Department of Obstetrics and Gynecology, Peking University Third Hospital; National Clinical Research Center for Obstetrics and Gynecology (Peking University Third Hospital); National Center for Healthcare Quality Management in Obstetrics, 100191, Beijing, China.

E-mail addresses: wangwei83427@bjmu.edu.cn (W. Wang), bysychenlian@126.com (L. Chen), zhaoyangyu@bjmu.edu.cn (Y. Zhao).

[1] Jiangxue Qu and Hai Jiang served as co–first authors and contributed equally to this work.

[2] Yangyu Zhao, Lian Chen, and Wei Wang served as co–corresponding authors and contributed equally to this work.

https://doi.org/10.1016/j.redox.2025.103530
Received 23 December 2024; Received in revised form 29 January 2025; Accepted 3 February 2025
Available online 8 February 2025

In summary, abnormal oxidative stress at the maternal-fetal interface induced the M1 polarization of decidual macrophages, causing the secretion of pro-inflammatory cytokines. TNF-α and IL-8 acted on uSMCs to inhibit CAP expression, inducing atonic PPH.

1. Introduction

Postpartum hemorrhage (PPH) is a common complication in obstetrics and is defined as blood loss exceeding 500 mL within 24 h of vaginal delivery [1]. PPH is the leading cause of pregnancy-related deaths and accounts for approximately a quarter of maternal deaths [2,3], which is correlated with the occurrence of adverse clinical outcomes [1]. Uterine atony is the most common cause of PPH (approximately 70 %) [4]. However, low-risk pregnant women experience atonic PPH in clinical settings. The vague mechanism and unpredictability of PPH cause delayed treatment and an increased risk of adverse clinical outcomes. Therefore, elucidating the mechanism of atonic PPH is crucial for identifying effective treatment measures.

As the uterus remodels in preparation for delivery, the excitability and contractility of the uterine smooth muscle layer, the myometrium, increases drastically [5]. At term, the increased secretion of pro-inflammatory cytokines (interleukin (IL)-8, tumor necrosis factor (TNF)-α, IL-1β, and IL-6) promote increased expression of cyclooxygenase-2 (COX-2) and oxytocin receptor (OTR) in myometrium; this results into strong and frequent uterine contractions, which subsequently promote the onset of labor [6]. The immune-inflammatory reaction at the maternal–fetal interface is crucial in this process, with decidual immune cells playing a crucial role in regulating the process. Decidual macrophages are the second largest immune cells at the maternal-fetal interface, accounting for 10–20 % [7]. Decidual macrophages transform into a pro-inflammatory phenotype at the onset of labor, inducing myometrium contraction and labor initiation [8]. Simultaneously, the levels of pro-inflammatory cytokines (TNF-α, IL-6, IL-1β, and C C motif ligand 2 (CCL-2) are positively correlated with uterine contractility [9–13].

However, some studies revealed that prolonged exposure to pro-inflammatory cytokines, including TNF-α and IL-1, could cause impaired oxytocin signaling and depletion of calcium ions in muscle cells, affecting uterine muscle contraction [10,11]. This suggested that excessive activation of immune-inflammatory responses might inhibit myometrium contraction. Previous studies demonstrated that the levels of immune-inflammatory factors, such as IL-1β, IL-18, macrophage inflammatory protein (MIP)-1α, IL-6, and monocyte chemotactic protein (MCP)-1, in the peripheral blood of pregnant women before delivery, who had atonic PPH, were significantly higher than those in the control group [4,14]. Consequently, the abnormal pro-inflammatory phenotype of decidual macrophages might affect the contractile function of uterine smooth muscle cells (uSMCs). The uterine blood flow at term pregnancy can be as high as 1300 ml/min. When the myometrium cannot contract in a strong and sustained manner, it fails to timely compress the spiral arteries that supply the placental bed, resulting in a rapid hemorrhage from the placental bed, culminating in the occurrence of PPH [15].

Previous studies have shown that the macrophage phenotype was closely related to their oxidative stress state. Mitochondrial damage and the release of excess oxidative substances, such as reactive oxygen species (ROS), were crucial for the release of pro-inflammatory cytokines in monocytes and macrophages [16]. Therefore, we aimed to investigate the relationship between immune-inflammatory and oxidative stress states in decidual macrophages at the maternal-fetal interface in atonic PPH. Similarly, we combined omics and multiplex Luminex assays to validate the promotion of M1 macrophage polarization and pro-inflammatory cytokine release through an abnormal oxidative stress state in decidual macrophages and the regulation of uSMC contraction to reveal the potential mechanism of atonic PPH which was confirmed through *in vitro* cell experiments and rat models.

2. Materials and methods

2.1. Inclusion criteria of clinical sample

This was a nested case-control study on a prospective cohort of pregnant women who underwent regular prenatal checkups at Peking University's Third Hospital between December 2022 and December 2023. The inclusion criteria were natural conception, full-term pregnancy, and single pregnancy through vaginal delivery. The exclusion criteria were PPH secondary to definite causes (such as placenta accreta, soft birth canal lacerations, underlying coagulation disorder, previous autoimmune diseases, and recent acute and chronic intrauterine or systemic infections), obstetric complications (including preeclampsia and gestational diabetes mellitus (GDM) other than type A1), and uterine atony with definite causes (such as macrosomia, multiple pregnancies, and precipitous deliveries). Following the above criteria, 30 pregnant women with PPH were included. The control (non-PPH) group was matched with baseline information (including maternal age, gestational age, and pregnancy complications, such as hypertensive disorders in pregnancy [HDP] and GDM) without PPH. All procedures were approved by the Medical Science Research Ethics Committee of Peking University Third Hospital (M2021685).

2.2. Clinical sample collection

Upon entering the first stage of labor (the interval between the onset of labor and complete or 10 cm cervical dilation), 5 mL of peripheral blood was collected in an Ethylenediaminetetaracetic acid (EDTA) tube. At the end of the third stage of labor, after placenta delivery, 5 mL of vaginal blood was collected in an EDTA tube. Both blood samples were centrifuged at 12,000×*g* and 4 °C for 10 min and stored at −80 °C.

Following the delivery of the placenta, 3 × 3 × 1 cm decidua and placental tissue were sectioned and fixed in 10 % neutral formalin. Subsequently, 5–10 g of decidua was scraped from the maternal surface of the placenta and washed with phosphate-buffered saline. The decidua tissue was then cut and digested in 100U/mL collagenase II and IV, and 100U/mL DNAase and placed on a constant temperature shaker at 37 °C for 40 min. The tissue was then ground on a 100 μm sieve. The resultant cell suspension was collected and then centrifuged at 1500 rpm for 5 min. After discarding the supernatant, 3–5 mL of ACK red blood cell (RBC) lysis buffer was added to lyse RBC at 4 °C for 10 min, and upon completion of lysis, 40 mL phosphate buffer saline (PBS) was added to terminate the process. After the decidual cells were centrifuged at 1500 rpm for 5 min, they were collected into 24-well plates at 3×10^6 cells per well for 24 h and centrifuged at 1500 rpm for 5 min. Finally, the supernatant, namely, the decidual cells culture medium, was collected.

Decidua samples were collected from women with normal vaginal delivery, and flow cytometry was used to select CD14+macrophages from the decidua. The decidual tissue was digested to extract decidual macrophages, and RBCs were lysed as described above, with the resultant cell suspension being collected for subsequent analysis. Flow cytometry was performed in a 100 μL system with 1 μL of CD14-APC antibody/2 * 10^6 cells for 20 min. The sorted cells were resuspended in a Dulbecco's Modified Eagle Medium (DMEM, Gibco, CAT: C11995500BT) containing 2 mmol/L glutamine and 25 ng/mL granulocyte-macrophage colony stimulating factor (GM-CSF) and collected in 48-well plates, specifically at $3.5*10^5$ cells per well.

2.3. Flow cytometry

2.3.1. Treatment of cells

The decidua samples from control group (CTRL) and atonic PPH patients were collected and processed as outlined in the section **Clinical sample collection.** Decidual cells were sorted, including macrophages, natural killer (NK) cells, and T lymphocytes (T cells) from the atonic PPH and CTRL groups.

Peripheral blood samples were collected from women with normal vaginal delivery during labor and centrifuged at 12,000×*g* for 10 min. The white membrane layer, including peripheral blood mononuclear cells, were collected through centrifugation with 3 mL of Ficol added. After being labeled with CD14 magnetic beads, $CD14^+$ monocytes were sorted using the Meitianni fully automatic magnetic bead sorter and then plated and cultured in 48-well plates at 4×10^5 cells per well for 24 h. The culture media were replaced with CTRL- or PPH-patient-derived decidual cells culture medium as outlined in the section **Clinical sample collection**. CD14+monocytes were further cultured for 48 h, and after centrifugation at 500×*g* for 5 min, the CD14+monocytes were collected for subsequent analysis.

Decidua samples were collected from women with normal vaginal delivery, and flow cytometry was used to select CD14+macrophages from the decidua, which was described comprehensively in the section **Clinical sample collection**. Decidual $CD14^+$ macrophages were plated and cultured in 48-well plates at 3.5×10^5 cells per well for 24 h, and 0, 1, 10, and 100 μmol/L of H_2O_2 were added for 1 h or cultured in the CTRL- or PPH-patient-derived decidual cell culture media for 48 h, followed by centrifugation at 500×*g* for 5 min. Finally, CD14+monocytes were collected for subsequent analysis.

2.3.2. Analyses

The decidual cells, including macrophages, NK cells, and T cells, were stained for 30 min at 25 °C in the dark. The following antibodies were used: Brilliant Violet 421 anti-human CD45 (Biolegend, CAT: 304032, dilution: 1:200), APC anti-human CD14 (Biolegend, CAT: 325608, dilution: 1:200), PE/Cyanine5 anti-human CD3 (Biolegend, CAT: 317355, dilution: 1:200), FITC anti-human CD56 (Biolegend, CAT: 362546, dilution: 1:200), and Mito SOX (Thermo, CAT: M36008, dilution: 1:500). The samples were then centrifuged at 1500×*g* for 5 min, washed and resuspended in 300–400 μL PBS. Finally, the cells were then immediately analyzed using a Canto flow cytometer (Beckman Counter FACS Galios).

The $CD14^+$ monocytes from peripheral blood samples were stained for 30 min at 25 °C in the dark. The following dyes were used: Mito SOX (Invitrogen, CAT: M36007, dilution: 1:2500) and DCFH-DA (Solarbio, CAT: D6470, dilution: 1:500). A SONY ID7000 full-spectrum flow cytometer was used to detect fluorescence.

The $CD14^+$ macrophages from decidual samples were stained for 1 h at 4 °C with 50 μL of staining system. The following antibodies were used: CD206 (Biolegend, CAT: 321131, dilution: 1:200) and CD86 (Biolegend, CAT: 374216, dilution: 1:200). Finally, upon completion of staining, the cells were immediately analyzed using a Beckman Cytoflex flow cytometer.

2.4. Vaginal proteomics

The vaginal blood was centrifuged at 12,000×*g* and 4 °C for 10 min. Subsequently, 50 μL of blood samples were incubated in magnetic nanomaterials (PTM-00F13303, PTM Bio) at 1200×*g* and 37 °C for 1 h, and magnetic beads were washed thrice. Next, 70 μL of enzymatic hydrolysis buffer (200 mM Tris,pH8.0) was added, followed by heating at 95 °C for 10 min. After the sample dropped to 25 °C, 20 ng/μL trypsin was added for hydrolysis overnight at 37 °C. To achieve a final concentration of 5 mM, reduction was performed at 56 °C for 30 min using 1 M dithiothreitol. Furthermore, 550 mM iodoacetamide was added to achieve a final concentration of 11 mM. According to the C18 ZipTips manual, salt was removed, and vacuum-freezing was conducted, followed by drying and liquid chromatography-mass spectrometry. After enzymatic hydrolysis, the peptide segments were acidified with 10 % trifluoroacetic acid to attain pH 2–3 and centrifuged at 12,000×*g* for 10 min at 25 °C, and the supernatant was collected. Similarly, 50 μL of activation solution, desalination solution, peptide segment, and desalination solution were added to StageTip sequentially, centrifuged at 1500×*g* per step for 1 min, and repeated once. Finally, 20 μL of eluent was added, followed by centrifugation at 750×*g* for 1 min, freezing, spin-drying, and setting aside for later use.

The peptide segments were dissolved in liquid chromatography mobile phase A and separated using an EASY nLC 1200 ultra-high-performance liquid chromatography system. For ionization, the samples were injected into an NSI ion source and analyzed using an Orbitrap Exploris 480 mass spectrometer. Data were collected using a data-independent scanning program. The intensity (I) of proteins in different samples was normalized through a centralization transformation to obtain the relative quantitative values (R) in different samples. To evaluate the quantitative reproducibility between biological or technological replicates, repeatability was analyzed using three statistical methods, namely Pearson's correlation coefficient, principal component analysis (PCA), and relative standard deviation (RSD).

2.5. Vaginal blood metabolomics

To 20 % acetonitrile methanol internal standard extraction solution, 50 μL of the sample was added, vortexed for 3 min, and centrifuged at 12,000×*g* and 4 °C for 10 min. The supernatant was stood at −20 °C for 30 min, centrifuged at 12,000×*g* and 4 °C for 3 min, and transferred for analysis on the machine. Raw data were extracted and corrected using the XCMS program in mzXML format. Metabolite identification was performed by searching the laboratory's in-house database and integrating public and prediction databases, and metDNA methods. Finally, substances with a comprehensive identification score of ≥0.5 and a QC sample CV of <0.3 were extracted, and the positive and negative modes were merged to obtain metabolite data.

We conducted quality control analysis, PCA, cluster analysis, grouped principal component analysis, orthogonal partial least squares discriminant analysis, dynamic distribution of metabolite content differences, and screening of differential metabolites. Metabolites with a variable importance in the projection (VIP) of >1 (Student's t-test, $P < 0.05$) were further analyzed. A higher VIP value indicated that a metabolite played a more prominent role in distinguishing between different groups or in explaining experimental variables. These metabolites may help elucidate or distinguish the differences between the groups effectively. In differential metabolite analysis, the Kyoto Encyclopedia of the Genome (KEGG), Human Metabolome Database (HMDB), and MebaboAnalyst databases were used for KEGG, HMDB, and MSEA functional annotation and enrichment analyses, respectively.

2.6. Proteomic and metabolomic analysis

Firstly, statistical analysis of differential proteins and metabolites was conducted. Specifically, the differential screening criteria for proteins were FC > 1.5 or FC < 1/1.5 and $P < 0.05$, whereas that for metabolites were | log2FC |>0, $P < 0.05$, and VIP>1. iPath analysis tools were used to simultaneously map differentially expressed proteins and metabolites to the iPath pathway map, obtain their shared pathway information, screen for pathways with both differential proteins and metabolites, and finally visualize them. Using the resultant quantitative outputs, the Spearman correlation analysis was performed on differentially expressed proteins and metabolites to screen for those that exhibited a significant correlation (correlation coefficient |r |≥0.8) and construct their co-expression relationship network. Finally, the Metscape plugin in Cytoscape was used to construct a network of differentially expressed proteins and metabolites. This network was built based

on secondary data from various sources (i.e., databases, experiments, etc.), delving into the relationship between metabolites and proteins. The compound network was visualized it displayed information on compound structures, reaction types, enzymes, genes, and pathways, while also being able to validate differential proteins at a metabolic level closer to phenotype. The above analysis combined methods commonly used in omics, including (1) association analysis based on statistical methods, (2) association analysis based on metabolic pathway analysis, (3) association analysis based on interaction, and (4) correlation analysis based on references and databases.

2.7. Multiplex Luminex assay

The extraction of decidual cell culture medium was described in the section **Clinical sample collection**. The decidual cells culture medium was centrifuged at 10,000×*g* for 10 min, 50 μL of which was taken for detection. Standard Diluent (250 μL) was added to the standard bottle, followed by ice bathing for 30 min and dilution of the standard curve. Microbeads were diluted with Assay Buffer, shaken, added (50 μL per well) to a 96-well plate, and washed thrice. A standard sample, sample, reference, and blank were added to the 96-well plate, shaken at 850×*g*, and incubated at 25 °C in the dark for 30 min. The sample was discarded, and the wells were washed thrice, followed by the addition of 25 μL of detection antibody to each well, shaking at 850×*g*, and incubation at 25 °C for 30 min in the dark. The detection antibody was discarded, and the wells were washed, followed by the addition of 50 μL of Streptavidin PE to each well, shaking at 850×*g*, incubation in the dark for 10 min, washing, the addition of 125 μL of assay buffer to each well, resuspension at 850×*g* and 25 °C away from light, and shaking for 30 s. The Luminex200 machine was used for value reading.

2.8. Cultivation of primary uSMCs

The primary uSMCs, purchased from Pricella, China (CP–H053), were cultured in the uSMCs culture medium (Pricella, China, CM-H053-125 × 4) with DMEM (Gibco, CAT: C11995500BT) containing 10 % fetal bovine serum (FBS) and 1 % antibiotic–antimycotic. Decidua samples were then collected from the normal delivery group (CTRL) and atonic PPH patients. The samples were digested as outlined in the section **Clinical sample collection** and decidual cells culture media were obtained. On the one hand, after the uSMCs were placed in 6 cm culture dishes ($1.5*10^6$ per dish), they were cultured in 3 mL decidual cell culture media from the CTRL and PPH groups for 24 h, respectively, and precipitates containing cells were obtained after digested with 0.5 % trypsin and centrifuged at 1000×*g* and 25 °C for 5 min. The uSMCs were used for subsequent Western blotting (WB), the details were outlined in the section **Western blotting (WB)**. On the other hand, decidual macrophages were obtained as described in the section **Clinical sample collection**. Decidual macrophages were cultured in 48-well plates at $3.5*10^5$ cells per well for 24 h. Then, 0, 1, 10, and 100 μmol/L of H_2O_2 were added to stimulate decidual macrophages respectively. After culturing for 1 h, the macrophage culture medium and macrophages were collected. Primary uSMCs were cultivated in mixed culture medium (1 mL macrophage culture medium containing 0, 1, 10, and 100 μmol/L of H_2O_2 and 2 mL uSMCs culture medium) for 1h. Finally, precipitates containing cells were obtained and used for subsequent WB as already described.

2.9. Immunofluorescence staining

Decidual tissues from the PPH and CTRL groups were fixed in 10 % neutral formalin for 48 h. The tissues were paraffin-embedded and cut into 5 μm sections for immunofluorescence staining (IF). The resultant paraffin sections were then deparaffinized and hydrated in xylene. Microwave thermal repair (Citric acid or EDTA repair solution was processed at 100 % power for 45 s. After the liquid boils, the decidual sections were added and then processed at 20 % power for 15 min). The sections were then cooled to 25 °C, washed, and incubated with PE blocking solution at 25 °C for 10 min. The decidual sections were then stained using primary antibody rabbit Vimentin mAb (Abcam, CAT: ab92547, dilution 1:200), rabbit CD14 mAb (Abcam, CAT: ab183322, dilution 1:100), rabbit CD56 mAb (Abcam, CAT: ab75813, dilution 1:1), and rabbit CD3 mAb (Abcam, CAT: ab16669, dilution 1:1). Secondary antibody incubation was performed using goat anti-mouse/rabbit (ZSGB-Bio, CAT: PV-6000) at 25 °C for 10 min. Tween (TBST) was rinsed for 2 min thrice, opal dye working solution was added dropwise (dilution concentration 1:100), and the corresponding channels (Vimentin-520, CD14-570, CD56-690, and CD3-620) were incubated at 25 °C for 10 min. Two drops of 4′,6-diamidino-2-phenylindole (DAPI) solution were added to 1 mL of Tris-HCl buffer solution and TBST and incubated at 25 °C for 5 min. A water-based sealing agent was used, followed by imaging using Phenoimager HT (Akita biosciences, U.S.A). After panoramic scanning imaging with a magnification of up to 20 × , the autofluorescence and stained fluorescence are separated using spectral splitting technology.

2.10. Immunohistochemistry

Decidual tissues from the PPH and CTRL groups and rat tissue sections (5 μm) were deparaffinized and rehydrated. After microwave thermal repair using pH 9.0 EDTA, mouse 8-OHdG mAb (Abcam, CAT: ab48508, dilution 1:100), rabbit SOD1 mAb (Abcam, CAT: ab51254, dilution 1:1000), rabbit SOD3 mAb (Abcam, CAT: ab171738, dilution 1:100), and rabbit anti GPX3 (Immunoway, CAT: YN1986, dilution 1:100) primary antibody working solutions were added to the tissues and incubated at 25 °C for 2 h. After microwave thermal repair using pH 6.0 citric acid, Rabbit recombinant multiclonal anti iNOS (Abcam, CAT: ab283655, dilution 1:1000) and rabbit CD206 mAb (CST, CAT: 24595, dilution 1:200) primary antibody working solutions were dropped onto the tissue at 37 °C for 2 h. 50–100 μL of secondary antibody goat anti-rabbit or mouse (ZSGB-Bio, CAT: PV-6001 or PV-6002) was added onto the tissue, incubated at 25 °C for 30 min, and washed in PBS. Diaminobenzidine was used as the working fluid for color development. Stained sections were then panoramic imaged using a Hamamatsu Digital Pathology Panorama Scanner (NanoZoomer A10) and analyzed using ImageJ software. Five fields of the same size for each section were selected blindly, brown-stained areas of fields were counted, and the average value was calculated.

2.11. Western blotting

We prepared 12.5 % and 5 % lower-layer separation and upper-layer concentrated gels, respectively. The lysates were resolved using sodium dodecyl sulfate-polyacrylamide gel electrophoresis, followed by 250 mA electro-transferring onto the nitrocellulose membrane, with a loading amount of 20 μg of protein. After sealing the membrane with 5 % BSA solution, incubation with the primary antibodies (overnight at 4 °C) and horseradish peroxidase-labeled secondary antibodies (1h at room temperature, dilution 1:3000) was performed sequentially. The primary antibodies used included anti-MMP2 (Abcam, CAT: ab92536, dilution 1:1000), anti-MMP9 (Abcam, CAT: ab76003, dilution 1:1000), anti-α-SMA (Abcam, CAT: ab5694, dilution 1:1000), anti-TAGLN (Abcam, CAT: ab170902, dilution 1:1000), anti-OTR (Abcam, CAT: ab300443, dilution 1:1000), anti-iNOS (Abcam, CAT: ab178945, dilution 1:1000), anti-Arg-1 (Abcam, CAT: ab133543, dilution 1:1000), anti-β-tubulin (abcam, CAT: ab133543, dilution 1:3000), and anti-β-actin (abcam, CAT: ab133543, dilution 1:3000). Next, the membrane was washed four times with 0.05 % TBST. The Tianneng system was used to visualize the outcomes. The grayscale value of the target strip was calculated using ImageJ software.

2.12. Enzyme-linked immunosorbent assay

Standard samples were diluted according to the manufacturer's instructions. Subsequently, the standard, control sample, and test sample were added to enzyme-linked immunosorbent assay (ELISA) 96 well plates coated with anti-TNF-α (R&D, CAT: DTA00D), IL-6 (R&D, CAT: D6050B), IL-8 (R&D, CAT: D8000C), and IL-10 (R&D, CAT: D1000B) antibodies, respectively. After incubation, the plates were washed, and ELISA antibodies were added. Finally, the substrate was colored, and absorbance was measured using an ELISA reader. Standard curves were drawn based on the concentrations of each dilution standard, and TNF-α, IL-6, IL-8, and IL-10 concentrations in the test sample were calculated.

2.13. Animal model

SD rats (9 weeks of age) were obtained from Beijing Vital River Laboratory Animal Technology Co., Ltd. (Beijing, China) and caged in a pathogen-free animal room with a 14 h light/10 h dark cycle. Gestational ages were determined by monitoring the formation of vaginal plugs (E0.5 = vaginal plug day). SD rats, including induced labor, non-induced labor, and non-pregnant groups, were intraperitoneally injected with different H_2O_2 concentrations at E19. At E20, the induced labor group received 0.5 mL of oxytocin and chloroprostol sodium via intramuscular injection, while the non-induced labor and non-pregnant groups did not receive induction drugs. Each group was further divided into three subgroups, namely ① Control (n = 11), ② 0.03 % H_2O_2 (n = 5), and ③ 0.15 % H_2O_2 (n = 5). H_2O_2 with a concentration of 30 % was obtained from the central laboratory of Peking University Third Hospital and diluted with sterile PBS to concentrations of 0.15 % and 0.03 %. The delivery process of pregnant rats was monitored after drug administration. After rats were sacrificed by inhalation drug method (carbon dioxide), placental, decidual, and uterine tissues were collected and placed in 10 % formaldehyde fixative or stored at −80 °C. An *in vitro* muscle strip contraction test was conducted to determine the range of uterine smooth muscle contractions in the pregnant rats. All rat experiments were approved by the Experimental Animal Ethics Committee of Peking University Third Clinical Medical College (A2023115).

Table 1
Clinical characteristics of pregnant women.

Characteristic	PPH (N = 30)	CTRL (N = 59)	t/χ^2	*P* value
Gestational age – w	39.74 ± 0.93	39.66 ± 0.95	0.376	0.708[a]
Maternal age – y	33.60 ± 3.43	32.44 ± 3.85	1.391	0.168[a]
Estimated blood loss - mL	849.33 (640.0, 1000.0)	237.12 (200.0, 300.0)	16.967	<0.001[b]
BMI before pregnancy - kg/m2	22.15 ± 2.98	21.02 ± 2.32	1.971	0.052[a]
Weight gain during pregnancy	14.76 (11.5, 18.0)	13.22 (10.6, 16.0)	1.648	0.103[b]
Way of conception			2.767	0.096[c]
Natural conception - No. (%)	19 (63.3 %)	47 (79.7 %)		
Assisted reproduction - No. (%)	11 (36.7 %)	12 (20.3 %)		
HDP - No. (%)	4 (13.3 %)	9 (15.3 %)	0.059	0.808[c]
GDM - No. (%)	6 (20.0 %)	12 (20.3 %)	0.001	0.970[c]
Spontaneous labor or induction			0.697	0.404[c]
Spontaneous labor - No. (%)	9 (30.0 %)	23 (39.0 %)		
Induction of labor - No. (%)	21 (70.0 %)	36 (61.0 %)		
Primiparous - No. (%)	22 (73.3 %)	45 (76.3 %)	0.092	0.761[c]
Previous intrauterine surgery - No. (%)	11 (36.7 %)	15 (25.4 %)	1.216	0.270[c]
Previous PPH - No. (%)	1 (3.3 %)	1 (1.7 %)	0.243	0.622[c]
Previous uterine diseases - No. (%)	7 (23.3 %)	13 (22.0 %)	0.019	0.890[c]
Fetal birthweight – g	3481.03 ± 327.74	3351.02 ± 281.35	1.929	0.057[b]
1min Apgar Score	29 (96.7 %)	58 (98.3 %)	0.243	0.622[b]

[a] Student's t-test.
[b] Mann–Whitney U test.
[c] Chi-square test; BMI, body mass index; HDP, hypertension disorders of pregnancy; GDM, gestational diabetes mellitus; w, week; y, year; CTRL, control group; PPH, atonic postpartum hemorrhage group.

2.14. Uterine smooth muscle tension detection

The Constant Temperature Smooth Muscle Trough (ZS-SX) and Madlab bioinformatics medical signal acquisition and processing system (Madlab-4C/5H) was purchased from Beijing Zhongshi Dichuang Technology Development Co., Ltd. 2 cm uterine smooth muscle tissue was collected and placed in Kerb's solution at 37 °C. A mixture of 95 % and 5 % O_2 and CO_2, respectively, was continuously administered. One end of the tissue was fixed to a tension transducer, and the contraction range of each group of uterine smooth muscles (myometrium) was measured in tension mode to obtain the contraction curve. Three waveforms were taken blindly from the contraction curve of each myometrium; the corresponding contractility was obtained by contraction of maximum muscle tension minus minimum muscle tension, and then the average value was taken to obtain the contractility of this myometrium.

2.15. Histological staining

Tissue samples from placentas and myometrium were collected and fixed in 10 % neutral-buffered formalin at 4 °C for 48 h. Tissues were paraffin-embedded and cut into 5 μm sections for hematoxylin-eosin staining (Leica Auto Stainer XL). Sections scanning was performed using a Hamamatsu Digital Pathology Panorama Scanner (NanoZoomer A10).

2.16. Transcriptome of rat tissue

The rat total RNA was extracted as per the instructions of the manufacturer, namely TRlzol Reagent (Life technologies, California, USA). RNA purity and concentration were detected using a NanoDrop 2000 spectrophotometer, and its integrity was characterized using an Agient2100/LabChip GX. Subsequently, the library was constructed: A total amount of 1 μg RNA per sample was used as input material for the RNA sample preparations. Sequencing libraries were generated using Hieff NGS Ultima Dual-mode mRNA Library Prep Kit for Illumina (Yeasen Biotechnology (Shanghai) Co., Ltd.) following the manufacturer's recommendations, and index codes were added to attribute sequences to each sample. Briefly, mRNA was purified from total RNA using poly-T oligo attached magnetic beads. First strand cDNA was synthesized, and second strand cDNA synthesis was subsequently performed. The remaining overhangs were converted into blunt ends via exonuclease/polymerase activities. After adenylation of 3′ ends of DNA fragments, NEBNext Adaptor with hairpin loop structure were ligated to prepare for hybridization. The library fragments were purified with AMPure XP system (Beckman Coulter, Beverly, USA). Then 3 μL USER Enzyme (NEB, USA) was used with size-selected, adaptor-ligated cDNA at 37 °C for 15 min followed by 5 min at 95 °C before PCR. Then, PCR was performed with Phusion High-Fidelity DNA polymerase, Universal PCR primers, and Index (X) Primer. Finally, PCR products were purified (AMPure XP system), and library quality was assessed using the Agilent Bioanalyzer 2100 system. The libraries were sequenced on an Illumina NovaSeq platform to generate 150 bp paired-end reads. The raw reads were further processed using a bioinformatic pipelinetool, BMKCloud (www.biocloud.net) online platform. Clean data (clean reads) were obtained by removing reads containing adapter, reads containing ploy-N and low quality reads from raw data. These clean reads were then mapped to the reference genome sequence (Rnor_6.0(*Rattus norvegicus*))

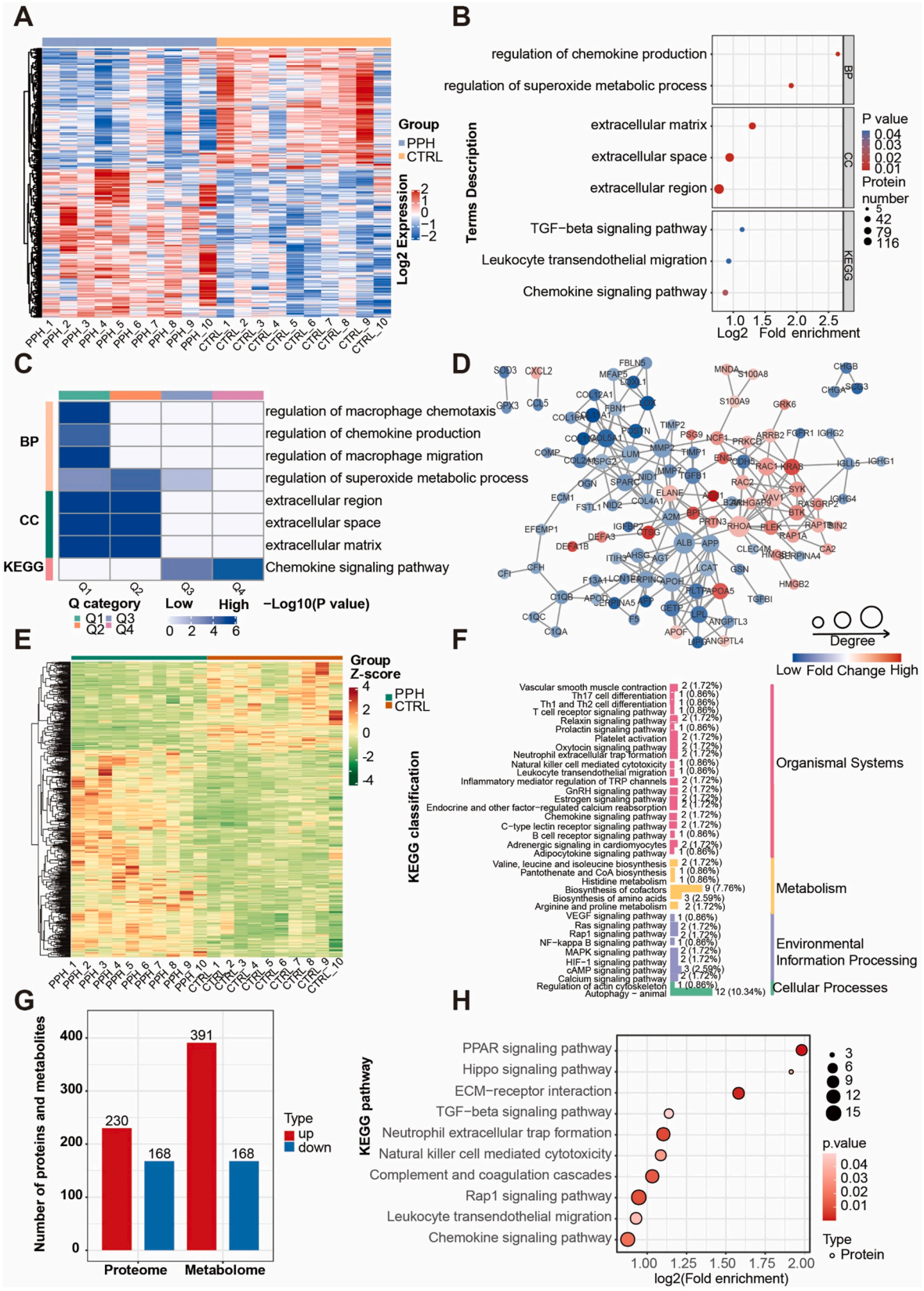

(caption on next page)

Fig. 1. Significant Differences in Proteins and Metabolites and Their Analysis Results (A) heatmap showing the clustering of differentially expressed proteins: columns and rows represent samples and differentially expressed proteins, respectively. Log2 conversion on the relative quantitative values was performed and was normalized by row (Z-score). The intensity of color indicates the expression level of the protein, specifically, the more intense the color, the higher the expression level; (B) and (C) KEGG enrichment pathway diagrams and GO enrichment pathway diagrams related to biological processes of significantly different proteins: (B) The graph shows eight significantly enriched functions, with the vertical axis representing GO functional description information and the horizontal axis representing the fold enrichment after Log2 conversion. The larger the value, the higher the degree of enrichment; the color of the dot represents the enrichment significance *P*-value, and the bluer or redder the color, the stronger the enrichment significance. The size of a dot represents the number of differentially expressed proteins in a specific GO function; specifically, the larger a dot, the greater the number of differentially expressed proteins nested within it. (C) To compare the functional similarities and differences between proteins with different expression levels, we divided the proteins into four parts based on their differential expression levels, called Q1 to Q4, enriched each part with GO and KEGG, and then performed functional clustering analysis. Clustering method: Based on Fisher's exact test *P*-value obtained from enrichment analysis, hierarchical clustering clusters the relevant functions in different Q groups together and draws a heatmap. The horizontal axis of the heatmap represents different Q groups, and the vertical axis represents the enriched related functions of differentially expressed proteins, such as the GO and KEGG pathways. The color blocks corresponding to the functional descriptions of different Q groups and differentially expressed protein enrichment indicate the level of enrichment significance. Blue represents high enrichment significance, while blue white represents low enrichment significance; (D) As shown in the differential protein interaction network, the circles in the figure represent differential proteins, and different colors represent the differential expression of proteins (blue represents downregulated proteins, red represents upregulated proteins). The darker the color, the greater the difference, and the size of the circles represents the number of proteins that interact with them; (E) Cluster analysis of differentially expressed metabolites, represented by a heatmap: Normalize the original relative content by row (Z-score), with the redder color indicating a higher relative content of the metabolite; (F) Enrichment pathways of significantly different metabolites. A bar chart categorizing the annotation results of differential metabolites KEGG according to KEGG pathway types: the number after the column represents the number of differential metabolites annotated to this pathway, while the percentage in parentheses represents the proportion of differential metabolites annotated to this pathway to the total number of metabolites annotated. The results of the joint analysis of metabolites and proteins with significant differences are presented in (G) and (H): (G) Histograms are used to display the distribution statistics of differentially expressed proteins and metabolites. The horizontal axis represents differential proteins or metabolites, and the vertical axis represents the number of differential proteins or metabolites. Blue represents the number of downregulated proteins, and red represents the number of up-regulated proteins; (H) As shown in the GO enrichment pathway diagram, the horizontal axis represents the enrichment factor of log2 conversion, and the vertical axis describes the KEGG pathway. The color of the dots represents enrichment significance, and red represents strong enrichment significance. The size of the dot represents the number of metabolites or proteins in the pathway.

by using Hisat2 tools soft. Gene function was annotated based on the following databases: non-redundant protein sequences (NCBI), Protein family (Pfam), Clusters of Orthologous Groups of proteins (KOG/COG), A manually annotated and reviewed protein sequence database (Swiss-Prot), KEGG, GO. Differential expression analysis of two samples was performed using the edgeR. The FDR <0.01 & Fold Change ≥ 2 was set as the threshold for significantly differential expression. GO classification and KEGG pathway enrichment analysis were conducted on differentially expressed genes in each group, and the GO and KEGG pathways were visualized.

2.17. Statistical analysis

Normality tests were performed for continuous variables. Using the Shapiro-Wilk test, estimated blood loss and weight gain during pregnancy were found to not be normally distributed ($P < 0.05$); therefore, the two indicators were described using their median (25th to 75th percentile). However, maternal and gestational age, body mass index (BMI), and fetal birth weight followed a normal distribution and were described as mean ± standard values. The student's t-test (for normally-distributed variables) or Mann–Whitney U test (for variables that are not normally-distributed) with continuous variables was used to evaluate the significance of inter-group differences. Categorical variables were expressed as numbers (percentages) and compared using the chi-squared test. Statistical analyses were conducted using SPSS (version 26.0; SPSS Inc., Chicago, Illinois, USA). Statistical significance was set at $P < 0.05$.

3. Results

3.1. Clinical sample information

Thirty pregnant women with atonic PPH and 59 matched controls were included in this study (Table 1). There were no statistically significant differences in maternal age ($P = 0.168$), gestational age ($P = 0.708$), BMI ($P = 0.052$), weight gain during pregnancy ($P = 0.103$), the proportion of assisted reproductive technology ($P = 0.096$), the proportion of induced labor ($P = 0.404$), the proportion of first childbirth ($P = 0.761$), pregnancy complications (GDM ($P = 0.970$) or HDP ($P = 0.808$)), fetal birth weight ($P = 0.057$), 1-min Apgar score ($P = 0.622$), previous uterine surgery history ($P = 0.270$), previous uterine disease history ($P = 0.890$), and previous PPH history ($P = 0.622$). However, the estimated blood loss of pregnant women in the PPH group was significantly higher than that in the control group ($P < 0.001$).

3.2. Abnormal immune-inflammatory state at the maternal-fetal interface in the PPH group may affect uterine smooth muscle contraction

We conducted proteomic (Fig. 1 A–D) and metabolomic (Fig. 1 E, F) analyses, as well as a joint omics analysis (Fig. 1 G, H), on vaginal blood samples from 10 pregnant women in the PPH and control groups. We identified and quantified 36,367 peptides and 4287 proteins, 4112 metabolites from vaginal blood. Compared with the control group, 230 and 168 significantly upregulated and downregulated proteins, and 391 and 168 significantly upregulated and downregulated metabolites were expressed in the PPH group, respectively (Fig. 1 G). The heatmaps for proteins and metabolites showed that the samples were well-aggregated within each group, indicating that the data quality met the analysis requirements (Fig. 1 A, E). GO and KEGG functional enrichment analyses revealed that the significantly differentially expressed proteins were primarily associated with immune-inflammatory functions, such as chemokine and cytokine production, and leukocyte functions, such as macrophage migration (Fig. 1 B, C). Moreover, complex interactions between proteins with significant differences in immune-inflammatory functions might influence the expression of CAPs, such as Matrix Metallopeptidase 2 (MMP2) (Fig. 1 D). We further identified significantly differentially expressed proteins detected in proteomics that were functionally associated with multiple immune cells (Fig. 2 A) and macrophages (Fig. 2 B). KEGG functional enrichment analysis showed that the significantly different metabolites were primarily involved in leukocyte migration, immune cell dysfunction, and relaxin and oxytocin signaling pathways (Fig. 1 F). In addition, we analyzed significantly different proteins and metabolites and discovered that the differentially expressed proteins and metabolites between the PPH and control groups were enriched in various immune cell functions, chemokines, and cytokine signaling pathways (Fig. 1 H).

We conducted 48 cytokine assays on decidual cell culture medium from five pregnant women in the PPH and control groups (Table 2). The results showed that compared with those in the control group, the concentrations of pro-inflammatory cytokines, such as TNF-α, IL-6, IL-

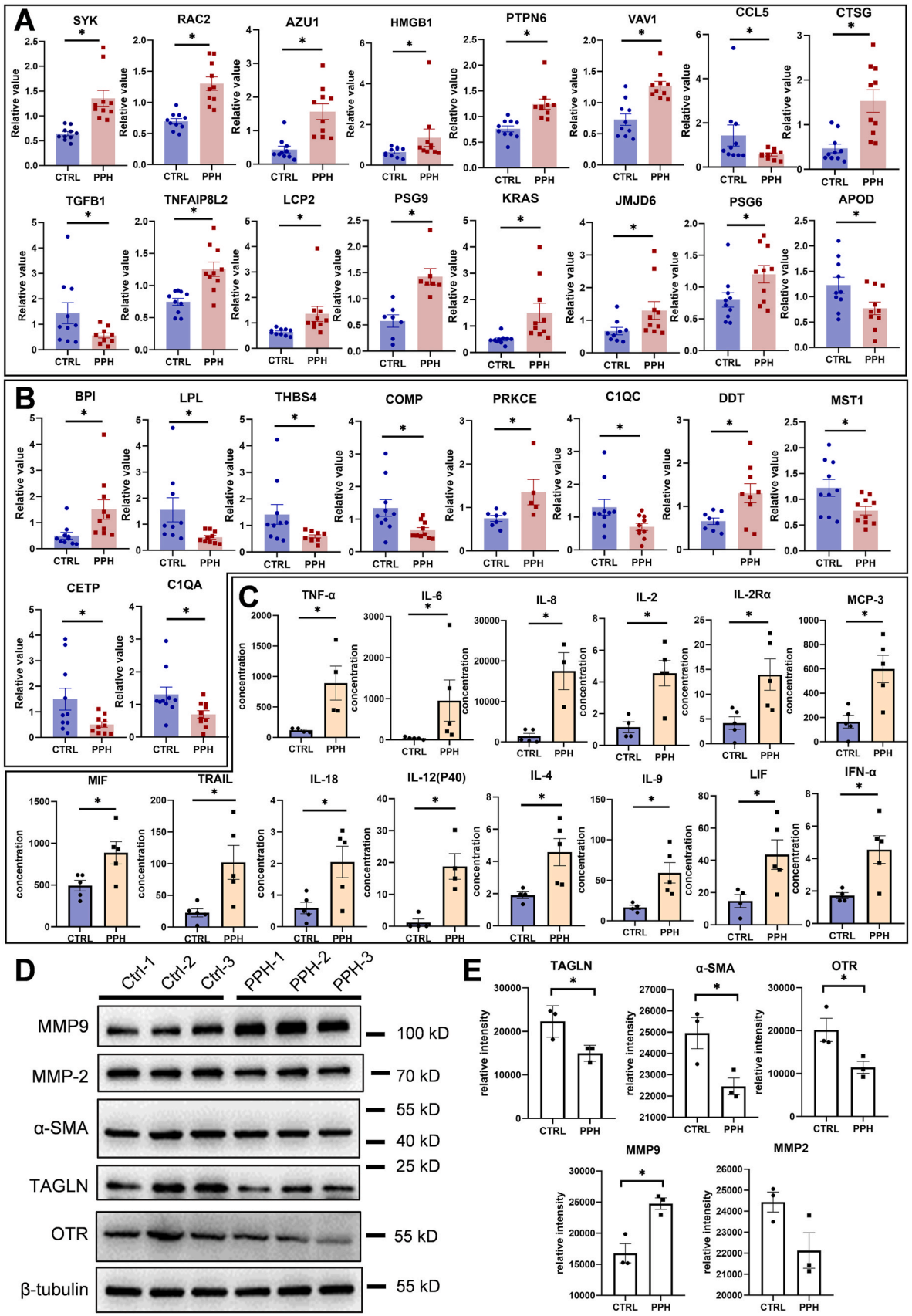

(caption on next page)

Fig. 2. Immune-related differential proteins in proteomics, detection results of cytokines in decidua culture medium, and their effects on the expression of contractile proteins in uterine smooth muscle cells (A) The boxplot shows the significantly differentially expressed proteins associated with multiple immune cells in the PPH group from proteomics; (B) The boxplot shows the significantly differentially expressed proteins associated with macrophages in the PPH group from proteomics; (C) The boxplot shows the significantly differentially expressed pro-inflammatory cytokines in the decidua culture medium of the PPH group; (D) The WB plot shows the expression of contraction-associated proteins (MMP2, MMP9, α-SMA, TAGLN and OTR) in primary uterine smooth muscle cells cultured in PPH and control group decidua culture medium, with β-tubulin as the reference; (E) The graph shows the quantitation of relative intensity of WB indicators. The data is expressed as mean ± standard deviation; *indicate the statistical difference between two groups. WB, Western blotting; MMP2, Matrix Metallopeptidase 2; MMP9, Matrix Metallopeptidase 9; α-SMA, α-Smooth muscle actin; TAGLN, Transgelin; OTR, Oxytocin Receptor; CTRL, control group; PPH, atonic postpartum hemorrhage group.

18, IL-2, IL-2Rα, MCP-3, MIF, tumor necrosis factor-related apoptosis-induced ligand (TRAIL), IL-8, IL-12 (p40), IL-4, IL-9, leukemia inhibitory factor (LIF), and interferon (IFN)-α in the pregnant women in the PPH group were significantly increased ($P < 0.05$) (Fig. 2 C). In addition, we cultured primary uSMCs using a decidual cell culture medium from the PPH and the control groups. We found that compared with those in the control group, the expression levels of CAPs TAGLN (14972.46 ± 1837.23 vs. 22281.79 ± 3610.41, $P = 0.035$), α-SMA (22453.84 ± 681.01 vs. 24958.34 ± 1271.19, $P = 0.040$), and OTR (11442.45 ± 2442.46 vs. 20171.53 ± 4693.28, $P = 0.046$) in the uSMCs of the PPH group were significantly reduced. In contrast, MMP9 expression (24757.56 ± 1608.86 vs. 16773.83 ± 2667.74, $P = 0.011$) was significantly increased, which was statistically significant (Fig. 2 D, E). MMP2 expression (22129.34 ± 1458.21 vs. 24439.35 ± 827.57, $P = 0.075$) was decreased but not statistically significant (Fig. 2 D, E).

3.3. Decidual macrophages at the maternal-fetal interface play a crucial role in PPH

The proportions of macrophages, NK cells, and T cells in the decidua of pregnant women in the PPH and control groups were further analyzed. The results showed that compared with those in the control group, the proportion of macrophages in the decidua of the PPH group was markedly increased (11.75 ± 1.65 vs. 8.51 ± 3.59, $P = 0.013$), while there was no statistical difference in the proportion of NK cells (19.28 ± 29.20 vs. 14.95 ± 27.32, $P = 0.687$) and T cells (18.24 ± 4.68 vs. 16.82 ± 11.53, $P = 0.713$) (Fig. 3A, C). In the PPH group, the ratio of M1 to M2 macrophages was significantly increased (0.87 ± 0.51 vs. 0.28 ± 0.16, $P = 0.024$) (Fig. 3 B, D). Moreover, immunofluorescence staining and flow cytometry demonstrated consistency regarding the proportions of macrophages, NK cells, and T cells in the decidua (Fig. 3 E).

3.4. Functional abnormalities in decidual macrophages in PPH may be related to their abnormal oxidative stress status

The proteomic analysis of vaginal blood samples revealed that significantly different proteins were associated with superoxide anion radical metabolism (Fig. 1 B, C). Moreover, we identified significantly differentially expressed proteins associated with oxidative stress using proteomics (Fig. 4 A and Table 2), and the observation was validated through immunohistochemistry in the decidua. The results showed that compared with those in the control group, the expression of oxidative stress protein 8-hidroxy-2-deoxyguanosine (8-OHdG) (32.27 ± 35.51 vs. 12.64 ± 6.46, $P = 0.004$) was significantly upregulated, while the antioxidant stress proteins superoxide anion radical dismutase 3 (SOD3) (4.42 ± 6.27 vs. 53.84 ± 27.80, $P < 0.001$) and glutathione peroxidase 3 (GPX3) (22.92 ± 20.28 vs. 74.65 ± 32.71, $P < 0.001$) exhibited significantly downregulated expression. However, superoxide anion radical dismutase 1 (SOD1) (111.72 ± 12.12 vs. 68.45 ± 20.69, $P = 0.003$) was significantly upregulated in the decidua tissue of the PPH group (111.72 ± 12.12 vs. 68.45 ± 20.69, $P = 0.003$) (Fig. 4 B, C). We further analyzed the superoxide anion radical levels of macrophages, NK cells, and T cells in the decidua. The results showed that, compared with those in the control group, the superoxide anion radical levels of macrophages in the PPH group were markedly elevated, whereas there were no significant differences in those of NK and T cells (Fig. 4 D).

3.5. Abnormal oxidative stress at the maternal-fetal interface affected the polarization of decidual macrophages, promoting the secretion of pro-inflammatory cytokines

We collected decidual macrophages from control (CTRL) group and atonic postpartum hemorrhage (PPH) group patients for culture and obtained supernatant. Then, using flow cytometry, we sorted $CD14^+$ monocytes in peripheral blood and added them to the culture supernatant of decidual macrophages in CTRL and PPH groups for stimulation. We assessed M1 and M2 macrophage markers and ROS and superoxide anion radical levels. The results revealed that compared with those in the control group, the expression of inducible nitric oxide synthase (iNOS), a polarization marker of M1 macrophages, in $CD14^+$ monocytes was significantly increased after stimulated by the supernatant of the PPH group (PPH: 23635.40 ± 8729.52 vs. CTRL: 11485.25 ± 4285.28, $P = 0.047$), while that of arginase-1 (Arg-1), a polarization marker of M2 macrophages, was decreased (PPH: 23848.17 ± 11147.57 vs. CTRL: 45586.93 ± 24790.19, $P = 0.161$) (Fig. 5 A, B). Moreover, 2′,7′-Dichlorodihydrofluorescein diacetate (DCFH-DA) (PPH: 46347.28 ± 11486.17 vs. CTRL: 2018.05 ± 7410.79, $P = 0.009$) and mitochondrial superoxide indicator (Mito SOX) (PPH: 176.28 ± 45.23 vs. CTRL: 97.04 ± 26.75, $P = 0.004$) were notably increased in the $CD14^+$ monocytes of PPH group (Fig. 5 C, D).

Given the potential role of oxidative stress in macrophage polarization, decidual macrophages were extracted from normal delivery patients and stimulated with H_2O_2. The PPH group decidual macrophage culture supernatant was used as a positive control to assess M1 and M2 macrophage markers and cytokine secretion. The results demonstrated that compared with that in the blank group (0 μM H_2O_2), the expression ratio of M1 macrophage polarization marker cluster of differentiation 86 (CD86) to M2 macrophage polarization marker cluster of differentiation 206 (CD206) was significantly increased in the H_2O_2 stimulation group with concentration gradient (1 μM H_2O_2: 2.96 ± 1.71 vs. Blank: 0.92 ± 0.39, $P = 0.007$; 10 μM H_2O_2: 3.40 ± 1.80 vs. Blank: 0.92 ± 0.39, $P = 0.002$; 100 μM H_2O_2:2.42 ± 1.88 vs. Blank: 0.92 ± 0.39, $P = 0.044$) (Fig. 5 G, H). Moreover, this increase was consistent with the polarization trend of decidual macrophages cultured in a PPH medium (PPH: 2.34 ± 0.93 vs. CTRL: 1.68 ± 0.69, $P = 0.007$) (Fig. 5 E, F). The pro-inflammatory cytokines TNF-α (1 μM H_2O_2: 1469.80 ± 523.70 vs. CTRL: 969.06 ± 437.98, $P = 0.023$; 10 μM H_2O_2: 1583.04 ± 527.79 vs. CTRL: 969.06 ± 437.98, $P = 0.008$; 100 μM H_2O_2: 1372.76 ± 255.67 vs. CTRL: 969.06 ± 437.98, $P = 0.079$), and IL-8 (1 μM H_2O_2: 87218.56 ± 21877.09 vs. CTRL: 68080.48 ± 25793.50, $P = 0.073$; 10 μM H_2O_2: 90929.86 ± 20642.87 vs. CTRL: 68080.48 ± 25793.50, $P = 0.034$; 100 μM H_2O_2: 94169048 ± 26501.95 vs. CTRL: 68080.48 ± 25793.50, $P = 0.016$) secreted by H_2O_2-stimulated decidual macrophages showed increased expression levels, while the expression of the anti-inflammatory cytokine IL-10 was significantly decreased (1 μM H_2O_2: 90.40 ± 54.71 vs. CTRL: 463.85 ± 99.13, $P < 0.001$; 10 μM H_2O_2: 78.44 ± 56.89 vs. CTRL: 463.85 ± 99.13, $P < 0.001$; 100 μM H_2O_2: 35.32 ± 24.00 vs. CTRL: 463.85 ± 99.13, $P < 0.001$) (Fig. 5 I). The differences in IL-6 expression levels were not statistically significant (1 μM H_2O_2: 7931.37 ± 3263.64 vs. CTRL: 8016.79 ± 2783.30, $P = 0.940$; 10 μM H_2O_2: 6995.21 ± 3158.40 vs. CTRL: 8016.79 ± 2783.30, $P = 0.372$; 100 μM H_2O_2: 6013.12 ± 1796.01 vs. CTRL: 8016.79 ± 2783.30, $P = 0.089$) (Fig. 5 I). Next, we cultured primary uSMCs in an H_2O_2-stimulated decidual macrophage culture medium. The results showed that

Table 2
Concentration of cytokines during pregnancy between the atonic postpartum hemorrhage and non-postpartum hemorrhage group.

Cytokine	PPH (n = 5)	non-PPH (n = 5)	*P* value
Basic FGF	11.142 ± 3.275	4.094 ± 1.878	0.003
CTACK	19.560 ± 8.676	8.225 ± 3.170	0.044
Eotaxin	1.806 ± 1.064	0.573 ± 0.374	0.065
G-CSF	2337.666 ± 4057.252	251.254 ± 236.130	0.284
GRO-α	1992.804 ± 1462.219	84.800 ± 46.945	0.071
HGF	502.902 ± 365.262	196.240 ± 151.529	0.121
IFN-α	4.558 ± 1.906	1.720 ± 0.380	0.023
IFN-γ	57.518 ± 36.595	21.676 ± 20.540	0.093
IL-1α	27.562 ± 16.880	5.886 ± 4.301	0.024
IL-1β	11.270 ± 10.911	2.092 ± 0.864	0.142
IL-1ra	2013.444 ± 1164.329	938.190 ± 1072.229	0.167
IL-10	45.052 ± 67.290	3.868 ± 2.176	0.267
IL-12(p40)	18.783 ± 8.044	1.695 ± 3.250	0.008
IL-12(p70)	1.076 ± 0.443	0.500 ± 0.156	0.148
IL-16	102.334 ± 69.744	33.976 ± 33.086	0.083
IL-17	5.998 ± 3.286	2.040 ± 0.848	0.054
IL-18	2.050 ± 1.115	0.590 ± 0.406	0.025
IL-2	4.550 ± 1.792	1.143 ± 0.690	0.009
IL-2Rα	13.972 ± 7.092	4.168 ± 2.849	0.021
IL-3	0.858 ± 0.440	0.220 ± 0.122	0.014
IL-4	4.580 ± 1.892	1.910 ± 0.420	0.029
IL-6	243.220 ± 142.271	41.496 ± 30.149	0.018
IL-8	17501.573 ± 7935.311	1416.080 ± 1539.017	0.004
IL-9	59.370 ± 28.184	16.685 ± 5.265	0.021
IL-10	3025.880 ± 2814.576	918.633 ± 1616.340	0.228
LIF	43.578 ± 20.555	14.800 ± 8.077	0.035
M-CSF	8.432 ± 3.843	1.943 ± 1.090	0.014
MCP-1	290.520 ± 194.969	163.670 ± 73.952	0.211
MCP-3	598.886 ± 252.788	164.804 ± 116.456	0.008
MIF	885.388 ± 300.775	492.604 ± 141.812	0.030
MIG	976.682 ± 1000.193	145.388 ± 281.808	0.111
MIP-1α	222.548 ± 199.173	28.320 ± 40.230	0.065
MIP-1β	4583.062 ± 7775.394	222.608 ± 157.089	0.245
RANTES	227.626 ± 232.934	73.778 ± 53.100	0.242
SCF	10.958 ± 4.385	3.338 ± 2.179	0.008
SDF-1α	44.372 ± 24.207	11.140 ± 2.598	0.061
TNF-α	891.560 ± 558.809	117.273 ± 34.233	0.033
TNF-β	55.164 ± 27.057	15.930 ± 4.439	0.025
TRAIL	102.064 ± 60.130	22.502 ± 14.344	0.021
β-NGF	3.268 ± 1.935	1.047 ± 0.244	0.104
IL-35	52.772 ± 25.619	55.556 ± 12.516	0.869
TGF-β1	2355.954 ± 626.013	2803.278 ± 950.519	0.405
TGF-β2	626.086 ± 98.357	604.176 ± 83.798	0.714
TGF-β3	111.822 ± 42.603	100.808 ± 22.869	0.624

After the delivery of the placenta during labor, 5–10g of decidua is scraped from the surface of the maternal placenta, digested and cultured to obtain the culture supernatant for cytokine detection. Data are presented as Mean ± Standard error of measured concentrations (pg/mL). Cytokines concentrations below the detection limit throughout pregnancy are not shown in the table, including GM-CSF, IL-13, IL-15, IL-5.

Basic FGF, basic fibroblast growth factor; CTACK, cutaneous T cell-attracting chemokine; G-CSF, granulocyte-colony stimulating factor; GRO-a, growth-regulated oncogene-alpha; HGF, hepatocyte growth 9factor; IFN-α, interferon alpha; IFN-γ, interferon gamma; IL, interleukin; LIF, leukemia inhibitory factor; M-CSF, macrophage colony stimulating factor; MCP, monocyte chemotactic protein; MIF, migration inhibitor factor; MIG, monokine induced by IFN-g; MIP-1α, macrophage inflammatory protein-1 alpha; MIP-1β, macrophage inflammatory protein-1 beta; RANTES, regulate upon activation normal T cell expressed and secreted; SCF, stem cell factor; SDF-1α, stromal cell-derived factor 1α; stromal cell-derived factor-alpha; TNF-α, tumor necrosis factor-alpha; TNF-β, tumor necrosis factor-beta; TRAIL, tumor necrosis factor-related apoptosis-induced ligand; β-NGF, beta-nerve growth factor; PPH, postpartum hemorrhage. *P* value < 0.05.

compared with those in the control group, the expression levels of CAPs (MMP2, α-SMA, and OTR) in uSMCs were reduced in the H_2O_2- (1, 10, and 100 μM) treated group. However, direct stimulation of uSMCs with H_2O_2 (1 μM, 10 μM, and 100 μM) only had mild effect on CAP expression (Fig. 5 J).

3.6. Constructing the pregnant rat model of uterine atony using oxidant H_2O_2

In the induced and non-induced labor groups, inflammation infiltration was observed in the decidua and uterine muscle stimulated with H_2O_2, compared with the control group (Fig. 6a and Supplemental Figure1 A), and the uterine muscle contractility was significantly reduced (induced labor −0.03 % H_2O_2: 0.81 ± 0.89 vs. CTRL: 2.49 ± 1.19, $P < 0.001$; induced labor −0.15 % H_2O_2: 0.74 ± 0.78 vs. CTRL: 2.49 ± 1.19, $P < 0.001$; non-induced labor −0.03 % H_2O_2: 1.53 ± 0.54 vs. CTRL: 2.67 ± 0.86, $P = 0.001$; non-induced labor −0.15 % H_2O_2: 1.59 ± 0.64 vs. CTRL: 2.67 ± 0.86, $P < 0.001$) (Fig. 6 B, Supplemental Fig. 1 B and C). However, in the non-pregnant group, there was no inflammatory infiltration in the uterine smooth muscle after stimulation with H_2O_2 (Supplemental Figure1 A), and the uterine muscle contractility was not affected (non-pregnant −0.03 % H_2O_2: 3.33 ± 0.91 vs. CTRL: 2.24 ± 1.03, $P = 0.003$; non-pregnant −0.15 % H_2O_2: 2.50 ± 0.93 vs. CTRL: 2.24 ± 1.03, $P = 0.480$) (Supplemental Fig. 1 B, C). We determined the expression of the M1 and M2 macrophage markers (iNOS and CD206, respectively) in the placentas of the induced and non-induced labor groups. The results depicted that after H_2O_2 stimulation, M1 and M2 macrophages showed increased and decreased proportions, respectively, in the placenta (Fig. 6 C and Supplemental Figure2 A). We further conducted transcriptome analysis on each group's placenta and uterine muscle layers. The results showed that in the induced (Fig. 6 D and F, Supplemental Fig. 2 B and D) and non-induced (Supplemental Fig. 3 A, B) labor groups, the significantly differentially expressed genes in the placenta of the H_2O_2 stimulation group were enriched in oxidative stress activation pathways, such as redox reaction and peroxisome, as well as immune-inflammatory pathways, such as cytokine secretion and inflammation activation, compared with the control group. In the uterine smooth muscle of the induced (Fig. 6 E and G, Supplemental Fig. 2 C and E) and non-induced (Supplemental Fig. 3C and D) labor groups, the significantly differentially expressed genes were enriched in pathways affecting muscle contraction ability, such as the calcium ion signaling pathway, muscle contraction and generation, and energy metabolism.

4. Discussion

In our previous study, we found that pregnant women with unexplained atonic PPH had similar levels of peripheral blood cytokines in the first and second trimesters of pregnancy to those who gave birth normally; however, in term pregnancy, immune activation and significant changes in the expression levels of pro-inflammatory cytokines might occur [4]. This suggested that abnormal immune-inflammatory activation associated with the occurrence of unexplained atonic PPH may occur during labor, but its specific mechanism is still unclear. During labor, multiple immune cells are located in the decidua at the maternal-fetal interface [17,18], playing significant roles in maintaining myometrium contraction and preventing complications. Therefore, in this study, we conducted omics analysis and cytokine detection of the decidua at the maternal-fetal interface, as well as subsequent *in vitro* cell experiments and animal experiments to explore which immune cell dysfunction promotes the occurrence of uterine atony, and further investigate the potential mechanism of atonic PPH.

The vaginal blood can effectively reflect the condition of the maternal-fetal interface. Therefore, to explore the immune-inflammatory changes at the maternal-fetal interface during the occurrence of atonic PPH, we conducted proteomic and metabolomic analyses of vaginal blood samples from the PPH and matched control groups. Our combined omics indicated that pregnant women with unknown atonic PPH exhibited abnormal expression of immune-inflammatory proteins and metabolites at the maternal-fetal interface. These significantly differentially expressed proteins and metabolites were enriched in chemokine and cytokine production and leukocyte function pathways such

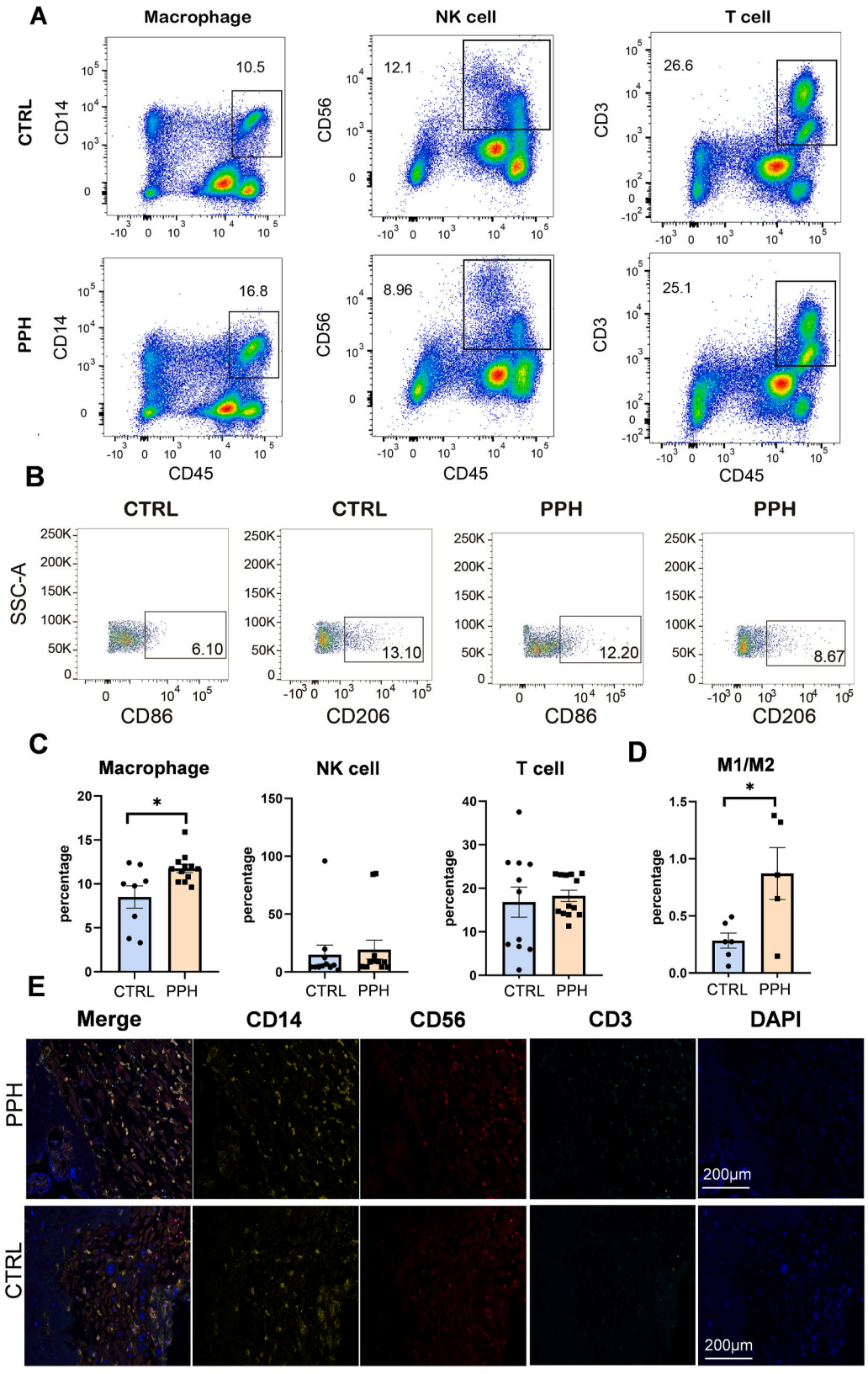

Fig. 3. Flow cytometry sorting results of decidual immune cell ratio between PPH group and control group (A) Flow cytometry images shows the proportion of macrophages, NK cells, and T cells in the decidua of the PPH group and the control group; (B) Flow cytometry images shows the proportion of M1 to M2 macrophages; (C) Statistical results of the proportion of macrophages, NK cells, and T cells; (D) Statistical results of the proportion of M1 to M2 macrophages; (E) The immunofluorescence images shows the proportion of macrophages, NK cells, and T cells in the decidua of the PPH group and the control group. Macrophages are marked with CD14, NK cells are marked with CD56, and T cells are marked with CD3; Scale bars, 200 μm, Ratio: 40 × . The data is expressed as mean ± standard deviation; * indicate the statistical difference between two groups. CTRL, control group; PPH, postpartum hemorrhage group.

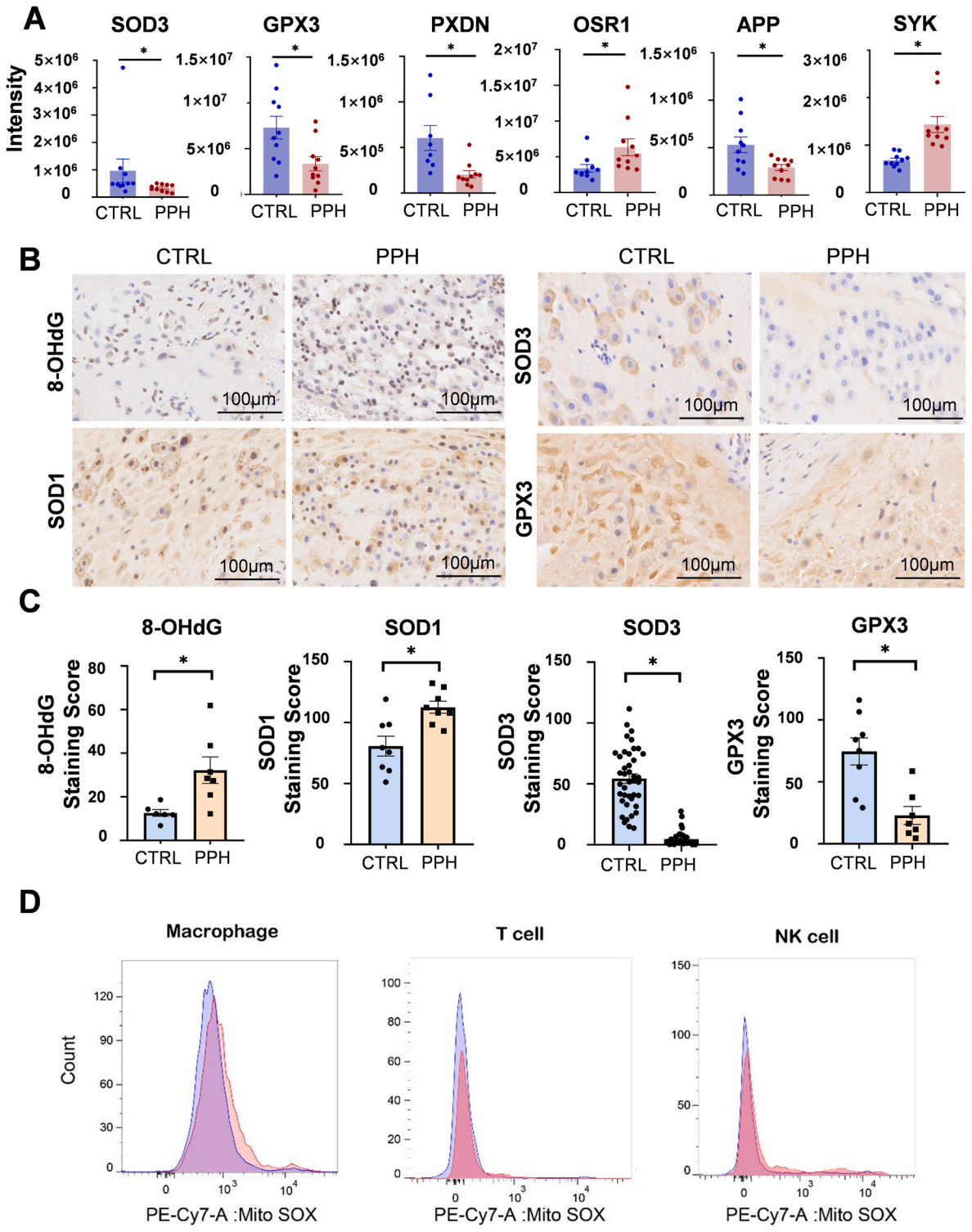

Fig. 4. Immunohistochemistry of decidual oxidative stress markers and flow cytometry results of superoxide anion radical levels in decidual immune cells between PPH group and control group (A) The boxplot displays significant differential proteins associated with oxidative stress in the PPH group of proteomics; (B) Immunohistochemical images shows the expression of 8-OHdG, SOD1, SOD3, and GPX3 in the decidua of the PPH group and the control group, Scale bars, 100 μm; (C) Statistical results of various indicators in immunohistochemistry; (D) The superoxide anion radical levels of macrophages, NK cells, and T cells in the decidua of the PPH group and the control group. Red represents the PPH group, blue represents the control group.
The data is expressed as mean ± standard deviation; * indicates the statistical difference between two groups. 8-OhdG, 8-hidroxy-2-deoxyguanosine; SOD,superoxide anion radical dismutase; GPX3,glutathione peroxidase 3; CTRL, control group; PPH, postpartum hemorrhage group.

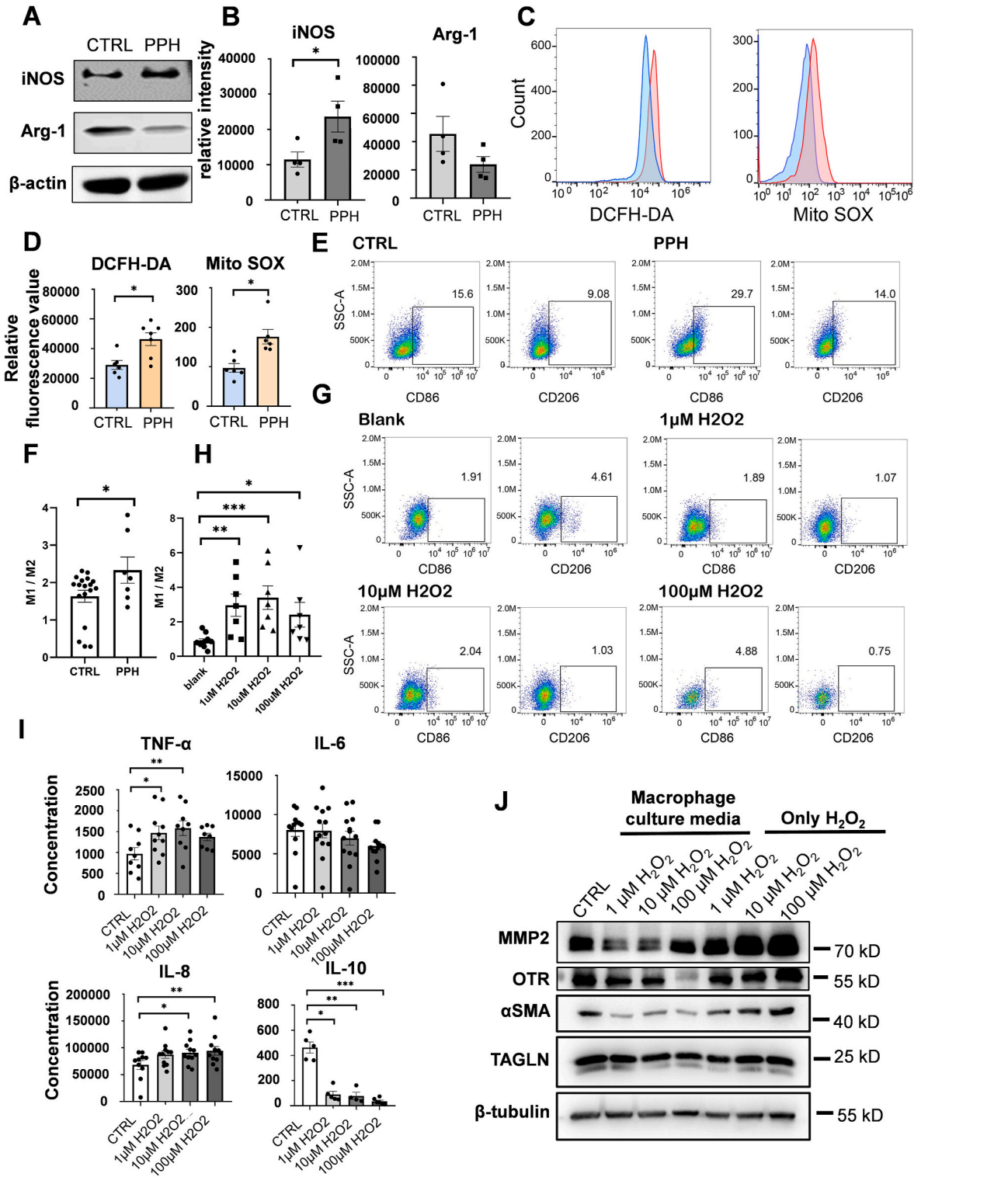

(caption on next page)

Fig. 5. Differences in oxidative levels and macrophage polarization between the PPH group and the control group, as well as changes in macrophage polarization, cytokine secretion, and effects on uterine smooth muscle contractility after H_2O_2 stimulation (A) The WB image shows the differential expression of M1 macrophage marker iNOS and M2 macrophage marker Arg-1 between the PPH group and the CTRL group, with β-actin as the reference; (B) The graph shows the quantitation of relative intensity of iNOS and Arg-1 in WB; (C) Flow cytometry images show the levels of ROS and superoxide anion radical between the PPH group and the CTRL group, with ROS labeled with DCFH-DA and superoxide anion radical labeled with Mito SOX. Red represents the PPH group, blue represents the control group; (D) The graph shows the quantitation of relative fluorescence value of ROS and superoxide anion radical levels in flow cytometry; (E) Flow cytometry image show the changes in the proportion of M1 to M2 macrophages after stimulation of decidual macrophages with PPH group and control group decidual culture medium, with CD86 as a marker for M1 macrophages and CD206 as a marker for M2 macrophages; (F) Statistical results of changes in the proportion of M1 to M2 macrophages after stimulation of decidual macrophages with PPH group and control group decidual culture medium; (G) Flow cytometry image show the changes in the proportion of M1 to M2 macrophages after H_2O_2 stimulation of decidual macrophages, with CD86 as a marker for M1 macrophages and CD206 as a marker for M2 macrophages; (H) Statistical results of changes in the proportion of M1 to M2 macrophages after H_2O_2 stimulation of decidual macrophages; (I) The boxplot show the secretion of cytokines by decidual macrophages stimulated by H_2O_2; (J) The WB image show the effect of using 1 μM, 10 μM, and 100 μM H_2O_2 to stimulate decidual macrophages in culture medium on the expression of CAPs in uSMCs. The reference protein is β-tubulin, with 1 μM H_2O_2, 10 μM H_2O_2, and 100 μM H_2O_2 representing the only H_2O_2 group, i.e., the expression of CAPs in uSMCs directly stimulated with 1 μM, 10 μM, and 100 μM H_2O_2. The data is expressed as mean ± standard deviation; * indicates the statistical difference between two groups. WB, Western blotting; iNOS, inducible nitric oxide synthase; Arg-1,arginase-1; ROS,reactive oxygen species; DCFH-DA, 2′,7′-Dichlorodihydrofluorescein diacetate; Mito SOX, mitochondrial superoxide indicator; CD86, cluster of differentiation 86; CD206, cluster of differentiation 206; CAPs, contractile associated proteins; MMP2,matrix metalloproteinase-2; α-SMA,alpha-smooth muscle actin; TAGLN, transgelin; OTR, oxytocin receptor; CTRL, control group; PPH, atonic postpartum hemorrhage group.

as macrophages. Our results showed a significant upregulation of pro-inflammatory cytokines at the maternal-fetal interface, indicating a high pro-inflammatory state at the maternal-fetal interface. Previous studies have suggested that uterine smooth muscle contraction could be promoted by moderate activation of the immune-inflammatory response and appropriate release of pro-inflammatory cytokines [19–21]. In contrast, uterine smooth muscle contraction might be inhibited by excessive activation and secretion of pro-inflammatory cytokines. For example, excessive expression of TNF-α and IL-1 could result in prolonged labor, excessive IL-6 expression could cause fetal descent arrest, and prolonged IL-1β exposure could cause impaired oxytocin signaling and calcium ion depletion in muscle cells, affecting uterine contractility [10,11]. These correspond with our research finding that in uterine smooth muscle contraction, excessive activation of immune inflammation at the maternal-fetal interface could affect the expression of proteins related to uterine smooth muscle contraction and oxytocin receptors, inhibiting uSMC contraction.

Multiple immune cells are at the maternal-fetal interface. We further investigated the immune cells majorly involved in atonic PPH. We discovered a severe imbalance in the proportion of decidual macrophages, with a significant increase in M1 to M2 macrophages. In previous studies, polarized macrophages are divided into M1 macrophages with pro-inflammatory properties and M2 macrophages with anti-inflammatory properties [7,22]. M1 macrophages produce pro-inflammatory factors, including TNF-α, IL-1 β, IL-6, and IL-8, while M2 macrophages produce anti-inflammatory factors, such as IL-10, with a strong immunosuppressive ability [23,24]. In this study, we also discovered that there are many pro-inflammatory cytokines related to macrophages, including TNF-α, IL-6, IL-8, IL-12 (p40), and IL-18, and factors related to macrophage chemotaxis and differentiation, such as MCP-3, MIF, and M-CSF, in the maternal-fetal interface of patients with atonic PPH.

Multiple biological processes regulated the function of decidual macrophages, and our results suggested that an imbalance in the proportion of decidual macrophages might be associated with abnormal oxidative stress at the maternal-fetal interface. At the maternal-fetal interface, patients with atonic PPH exhibited abnormal levels of oxidative stress in the decidual macrophages. The decidual culture medium in the PPH group stimulated peripheral blood mononuclear cells to polarize towards M1 macrophages and promoted increased intracellular ROS and superoxide anion radical levels. After stimulation with the oxidant H_2O_2, decidual macrophages polarized towards M1, and TNF-α and IL-8 expression levels were increased, which was similar to the high pro-inflammatory state of M1 at the maternal-fetal interface observed previously during the occurrence of atonic PPH. This is consistent with previous findings that the release of many ROS upregulated the macrophagic release of pro-inflammatory cytokines [25]. Previous studies on preterm birth have shown that inflammation and oxidative stress are risk factors for preterm birth [26]. With a premature shift in the maternal-fetal interface towards a pro-inflammatory environment and increased free radicals, premature activation of the delivery cascade and the occurrence of preterm birth might occur [27]. Disruption of immune tolerance and oxidative uterine-placental environment promoted the transformation of the uterine muscle layer from quiescent to active [28]. Similarly, we found that the expression of contraction proteins and oxytocin receptors was impaired in uSMCs cultured in a decidual macrophage culture medium stimulated with H_2O_2. An experiment in pregnant rats validated this hypothesis in animals. After stimulation with H_2O_2, the decidua polarized towards the M1 type, and the placenta showed excessive inflammation and abnormal gene expression related to oxidative stress and immune inflammation. Uterine smooth muscles showed decreased contractility and abnormal expression of genes related to muscle contraction, including the calcium ion signaling pathway, muscle contraction and generation, and energy metabolism.

Our study suggested that oxidative stress activation of decidual macrophages at the maternal-fetal interface promoted the polarization of decidual macrophages towards M1 macrophages, releasing pro-inflammatory cytokines, such as TNF-α and IL-8, which acted on uSMCs and inhibits contractility, resulting in atonic PPH. We are the first to explain the mechanism of atonic PPH caused by immune-inflammatory abnormalities related to oxidative stress, explore the relationship between vaginal blood and decidua at the maternal-fetal interface and uterine contractility, and creatively construct a pregnant rat model and related detection system for uterine atony. This broadens the research possibility on PPH mechanisms and provides new directions for further exploration of potential prevention and treatment measures.

CRediT authorship contribution statement

Jiangxue Qu: Writing – review & editing, Writing – original draft, Validation, Methodology, Data curation. **Hai Jiang:** Writing – original draft, Validation, Funding acquisition, Conceptualization. **Boyang Zhang:** Methodology, Data curation. **Huifeng Shi:** Methodology, Formal analysis, Data curation. **Shuai Zeng:** Resources, Methodology. **Wei Wang:** Writing – review & editing, Supervision, Investigation. **Lian Chen:** Supervision, Methodology, Conceptualization. **Yangyu Zhao:** Supervision, Funding acquisition, Conceptualization.

Declaration of competing interest

The authors declare the following financial interests/personal relationships which may be considered as potential competing interests: Yangyu Zhao reports financial support was provided by National Key

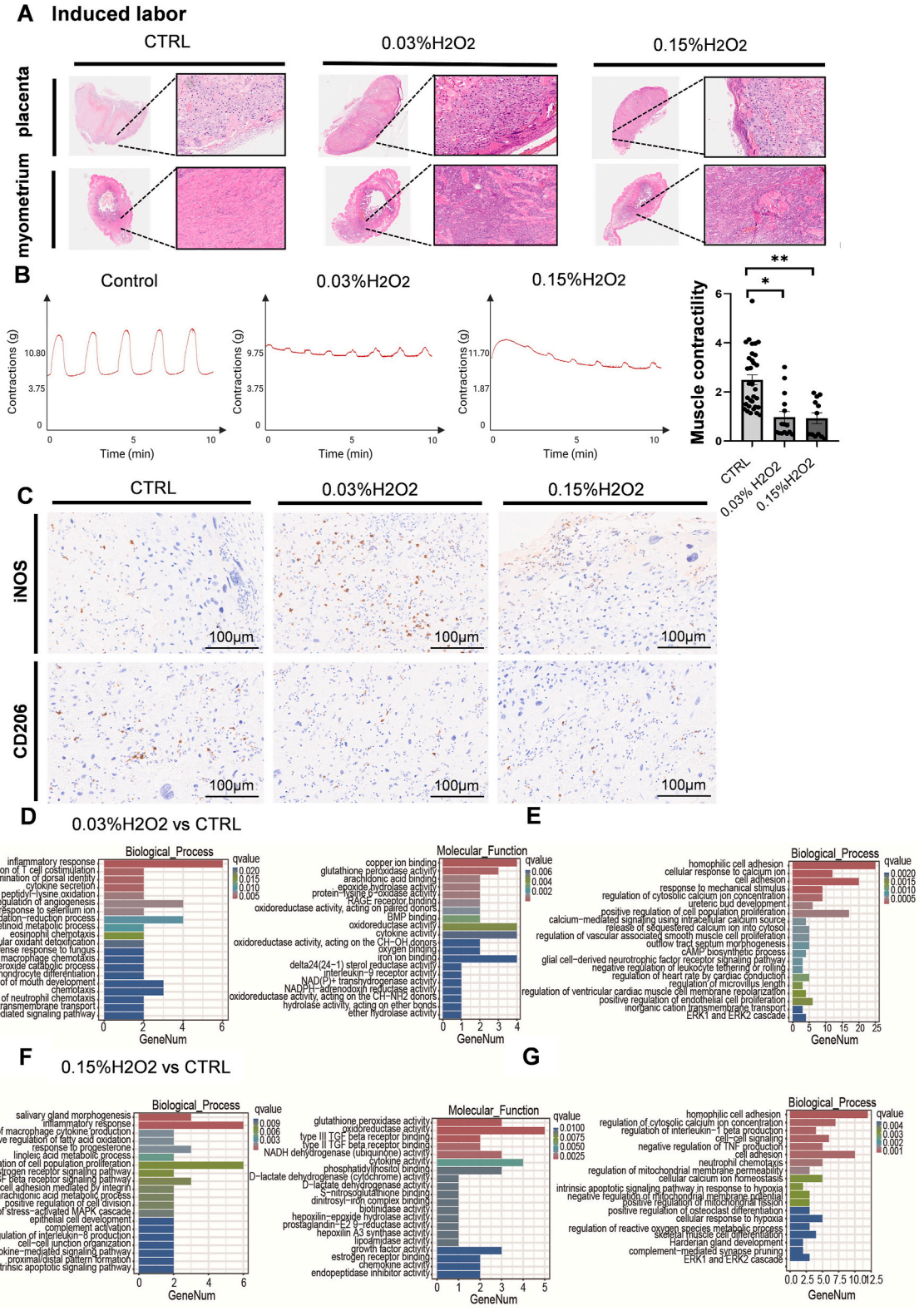

(caption on next page)

Fig. 6. Construction of uterine atony model induced by H_2O_2 stimulation in induced labor group of pregnant rats Pregnant rats were intraperitoneally injected with physiological saline (CTRL group), 0.03 % H_2O_2, and 0.15 % H_2O_2, followed by induction of labor using 0.5 mL oxytocin+0.5 mL chloroprostol sodium. The placenta and myometrium of each group of pregnant rats during delivery were collected. (A) H&E results of placental and myometrium of pregnant rats in CTRL group, 0.03 % H_2O_2 group, and 0.15 % H_2O_2 group; Ratio: 80 × . (B) Measurement of myometrium contractility in pregnant rats in CTRL group, 0.03 % H_2O_2 group, and 0.15 % H_2O_2 group, where the horizontal axis represents monitoring duration and the vertical axis represents contraction force (g). The statistical results of each group are shown in the bar chart. Muscle contractility refers to randomly selecting three waveforms from the myometrium detection chart, where the contraction force at each waveform is equal to the maximum force minus the minimum force, and then taking the average value; The points in the bar chart represent the number of repeated samples. (C) Immunohistochemical images showed the activation of M1 and M2 macrophages in the placental decidual layer of the 0.03 % H_2O_2 group, 0.15 % H_2O_2 group, and CTRL group. INOS is a marker for M1 macrophages, and CD206 is a marker for M2 macrophages; Ratio: 40 × , Scale bars, 100 μm; (D–G) The qvalue represents the significance of the functional pathway, and the smaller the qvalue, the more significant it is. The horizontal axis is GeneNum, which represents the number of genes of interest annotated in the entry, and the vertical axis represents each GO annotation entry or pathway entry. The color of the column represents the qvalue of the hypergeometric test: (D) GO images of transcriptome results of placenta in pregnant rats treated with 0.03 % H_2O_2; (E) GO images of transcriptome results of uterine smooth muscles in pregnant rats treated with 0.03 % H_2O_2; (F) GO images of transcriptome results of placenta in pregnant rats treated with 0.15 % H_2O_2; (G) GO images of transcriptome results of uterine smooth muscles in pregnant rats treated with 0.15 % H_2O_2.
The data is expressed as mean ± standard deviation; * indicates the statistical difference between two groups. CTRL, control group; PPH, atonic postpartum hemorrhage group.

Research and Development Program. Yangyu Zhao reports was provided by National Natural Science Foundation of China. Hai Jiang reports financial support was provided by China Postdoctoral Science Foundation. Hai Jiang reports financial support was provided by National Natural Science Foundation of China. If there are other authors, they declare that they have no known competing financial interests or personal relationships that could have appeared to influence the work reported in this paper.

Acknowledgements

We thank the patients who participated in this study. We would like to thank Editage (www.editage.cn) for English language editing. This study was funded by the National Key Research and Development Program (2021YFC2701500), National Natural Science Foundation of China (82271718), China Postdoctoral Science Foundation (2022M720296), National Natural Science Foundation of China (82301926) and International Institute of Population Health, Peking University Health Science Center.

Appendix A. Supplementary data

Supplementary data to this article can be found online at https://doi.org/10.1016/j.redox.2025.103530.

Data availability

Data will be made available on request.

References

[1] S. Hofer, J. Blaha, P.W. Collins, A.S. Ducloy-Bouthors, E. Guasch, F. Labate, F. Lança, L.T. Nyfløt, K. Steiner, M. Van de Velde, Haemostatic support in postpartum haemorrhage: a review of the literature and expert opinion, Eur. J. Anaesthesiol. 40 (1) (2023 Jan 1) 29–38, https://doi.org/10.1097/EJA.0000000000001744.
[2] S.E. Post, K.M. Rood, M.K. Kiefer, Interventions of postpartum hemorrhage, Clin. Obstet. Gynecol. 66 (2) (2023 Jun 1) 367–383, https://doi.org/10.1097/GRF.0000000000000785.
[3] GBD 2015 Maternal Mortality Collaborators, Global, regional, and national levels of maternal mortality, 1990-2015: a systematic analysis for the Global Burden of Disease Study 2015, Lancet 388 (10053) (2016 Oct 8) 1775–1812, https://doi.org/10.1016/S0140-6736(16)31470-2.
[4] H. Jiang, H. Shi, L. Chen, J. Yang, P. Yuan, W. Wang, Y. Pang, Y. Wei, Y. Zhao, Is there a relationship between plasma, cytokine concentrations, and the subsequent risk of postpartum hemorrhage? Am. J. Obstet. Gynecol. 226 (6) (2022 Jun) 835.e1–835.e17, https://doi.org/10.1016/j.ajog.2021.12.021.
[5] S. Wray, S. Arrowsmith, A. Sharp, Pharmacological interventions in labor and delivery, Annu. Rev. Pharmacol. Toxicol. 63 (2023 Jan 20) 471–489, https://doi.org/10.1146/annurev-pharmtox-051921-122822.
[6] H. Kobayashi, The entry of fetal and amniotic fluid components into the uterine vessel circulation leads to sterile inflammatory processes during parturition, Front. Immunol. 3 (2012 Oct 23) 321, https://doi.org/10.3389/fimmu.2012.00321.
[7] X. Jiang, L. Li, Decidual macrophage: a reversible role in immunotolerance between mother and fetus during pregnancy, Arch. Gynecol. Obstet. 309 (5) (2024 May) 1735–1744, https://doi.org/10.1007/s00404-023-07364-3.
[8] N. Gomez-Lopez, J. Galaz, D. Miller, M. Farias-Jofre, Z. Liu, M. Arenas-Hernandez, V. Garcia-Flores, Z. Shaffer, J.M. Greenberg, K.R. Theis, R. Romero, The immunobiology of preterm labor and birth: intra-amniotic inflammation or breakdown of maternal-fetal homeostasis, Reproduction 164 (2) (2022 Jun 20) R11–R45, https://doi.org/10.1530/REP-22-0046.
[9] E.R. Unal, J.T. Cierny, C. Roedner, R. Newman, L. Goetzl, Maternal inflammation in spontaneous term labor, Am. J. Obstet. Gynecol. 204 (3) (2011 Mar) 223.e1–223.e5, https://doi.org/10.1016/j.ajog.2011.01.002.
[10] J.T. Cierny, E.R. Unal, P. Flood, K.Y. Rhee, A. Praktish, T.H. Olson, L. Goetzl, Maternal inflammatory markers and term labor performance, Am. J. Obstet. Gynecol. 210 (5) (2014 May) 447.e1–447.e6, https://doi.org/10.1016/j.ajog.2013.11.038.
[11] J. Fitzgibbon, J.J. Morrison, T.J. Smith, M. O'Brien, Modulation of human uterine smooth muscle cell collagen contractility by thrombin, Y-27632, TNF alpha and indomethacin, Reprod. Biol. Endocrinol. 7 (2009 Jan 8) 2, https://doi.org/10.1186/1477-7827-7-2.
[12] Y. Jiang, L. Pin, W. Shi, Q. Huang, L. Wang, H. Liu, SAA1 regulates pro-labour mediators in term labour by activating YAP pathway, Mol. Cell. Biochem. 476 (7) (2021 Jul) 2791–2801, https://doi.org/10.1007/s11010-021-04125-1.
[13] Z. Chen, Q. Liu, Z. Zhu, F. Xiang, R. Wu, X. Kang, Toll-like receptor 4 contributes to uterine activation by upregulating pro-inflammatory cytokine and CAP expression via the NF-κB/P38MAPK signaling pathway during pregnancy, J. Cell. Physiol. 235 (1) (2020 Jan) 513–525, https://doi.org/10.1002/jcp.28991.
[14] D.M. Gallo, R. Romero, M. Bosco, T. Chaiworapongsa, N. Gomez-Lopez, M. Arenas-Hernandez, E. Jung, M. Suksai, F. Gotsch, O. Erez, A.L. Tarca, Maternal plasma cytokines and the subsequent risk of uterine atony and postpartum hemorrhage, J. Perinat. Med. 51 (2) (2022 Jun 21) 219–232, https://doi.org/10.1515/jpm-2022-0211.
[15] H.E. Miller, J.R. Ansari, Uterine atony, Curr. Opin. Obstet. Gynecol. 34 (2) (2022 Apr 1) 82–89, https://doi.org/10.1097/GCO.0000000000000776.
[16] R. Miao, C. Jiang, W.Y. Chang, H. Zhang, J. An, F. Ho, P. Chen, H. Zhang, C. Junqueira, D. Amgalan, F.G. Liang, J. Zhang, C.L. Evavold, I. Hafner-Bratkovič, Z. Zhang, P. Fontana, S. Xia, M. Waldeck-Weiermair, Y. Pan, T. Michel, L. Bar-Peled, H. Wu, J.C. Kagan, R.N. Kitsis, P. Zhang, X. Liu, J. Lieberman, Gasdermin D permeabilization of mitochondrial inner and outer membranes accelerates and enhances pyroptosis, Immunity 56 (11) (2023 Nov 14) 2523–2541.e8, https://doi.org/10.1016/j.immuni.2023.10.004.
[17] N. Gomez-Lopez, D. StLouis, M.A. Lehr, E.N. Sanchez-Rodriguez, M. Arenas-Hernandez, Immune cells in term and preterm labor, Cell. Mol. Immunol. 11 (6) (2014 Nov) 571–581, https://doi.org/10.1038/cmi.2014.46.
[18] K. Motomura, D. Miller, J. Galaz, T.N. Liu, R. Romero, N. Gomez-Lopez, The effects of progesterone on immune cellular function at the maternal-fetal interface and in maternal circulation, J. Steroid Biochem. Mol. Biol. 229 (2023 May) 106254, https://doi.org/10.1016/j.jsbmb.2023.106254.
[19] Z. Chen, Q. Liu, Z. Zhu, F. Xiang, R. Wu, X. Kang, Toll-like receptor 4 contributes to uterine activation by upregulating pro-inflammatory cytokine and CAP expression via the NF-κB/P38MAPK signaling pathway during pregnancy, J. Cell. Physiol. 235 (1) (2020 Jan) 513–525, https://doi.org/10.1002/jcp.28991.
[20] X. You, Z. Chen, H. Zhao, C. Xu, W. Liu, Q. Sun, P. He, H. Gu, X. Ni, Endogenous hydrogen sulfide contributes to uterine quiescence during pregnancy, Reproduction 153 (5) (2017 May) 535–543, https://doi.org/10.1530/REP-16-0549.
[21] B. Schmid, S. Wong, B.F. Mitchell, Transcriptional regulation of oxytocin receptor by interleukin-1beta and interleukin-6, Endocrinology 142 (4) (2001 Apr) 1380–1385, https://doi.org/10.1210/endo.142.4.8107.
[22] M. Orecchioni, Y. Ghosheh, A.B. Pramod, K. Ley, Macrophage polarization: different gene signatures in M1(LPS+) vs. Classically and M2(LPS-) vs. Alternatively activated macrophages, Front. Immunol. 10 (2019 May 24) 1084, https://doi.org/10.3389/fimmu.2019.01084.
[23] M.H. Mercnik, C. Schliefsteiner, H. Fluhr, C. Wadsack, Placental macrophages present distinct polarization pattern and effector functions depending on clinical

onset of preeclampsia, Front. Immunol. 13 (2023 Jan 12) 1095879, https://doi.org/10.3389/fimmu.2022.1095879.

[24] X.Q. Wang, W.J. Zhou, X.X. Hou, Q. Fu, D.J. Li, Correction: trophoblast-derived CXCL16 induces M2 macrophage polarization that in turn inactivates NK cells at the maternal-fetal interface, Cell. Mol. Immunol. 16 (3) (2019 Mar) 313, https://doi.org/10.1038/s41423-018-0194-9.

[25] W. Yu, X. Wang, J. Zhao, R. Liu, J. Liu, Z. Wang, J. Peng, H. Wu, X. Zhang, Z. Long, D. Kong, W. Li, C. Hai, Stat2-Drp1 mediated mitochondrial mass increase is necessary for pro-inflammatory differentiation of macrophages, Redox Biol. 37 (2020 Oct) 101761, https://doi.org/10.1016/j.redox.2020.101761.

[26] W. Deng, J. Cha, J. Yuan, H. Haraguchi, A. Bartos, E. Leishman, B. Viollet, H. B. Bradshaw, Y. Hirota, S.K. Dey, p53 coordinates decidual sestrin 2/AMPK/mTORC1 signaling to govern parturition timing, J. Clin. Investig. 126 (8) (2016 Aug 1) 2941–2954, https://doi.org/10.1172/JCI87715.

[27] L.S. Richardson, A.K. Kammala, S. Kim, P.Y. Lam, N. Truong, E. Radnaa, R. Urrabaz-Garza, A. Han, R. Menon, Development of oxidative stress-associated disease models using feto-maternal interface organ-on-a-chip, FASEB J. 37 (7) (2023 Jul) e23000, https://doi.org/10.1096/fj.202300531R.

[28] C.R. Manuel, M.S. Latuga, CR Jr Ashby, S.E. Reznik, Immune tolerance attenuates gut dysbiosis, dysregulated uterine gene expression and high-fat diet potentiated preterm birth in mice, Am. J. Obstet. Gynecol. 220 (6) (2019 Jun) 596.e1–596.e28, https://doi.org/10.1016/j.ajog.2019.02.028.